

# Spatial distribution of atoms in gas-covered Pd-X nanoparticles (X= Ag, Cu, Ni, Pt)

Mahesh Menon and Badal C. Khanra\*

Condensed Matter Physics Group, Saha Institute of Nuclear Physics

1/AF, Bidhannagar, Calcutta- 700 064, India

## Abstract

A Monte-carlo (MC) simulation procedure has been developed where the pair bond energies are allowed to take into account the various coordination numbers of surface atoms and the presence of adsorbates. The pair bond energies are calculated from partial bond energies of atoms which, in turn, are calculated from modified tight binding model in the second moment approximation. The model has been applied to study the role of adsorption of hydrogen, oxygen, carbon monoxide and nitric oxide on the surface composition and surface bond geometry of bimetallic Pd-X (X = Ag, Cu, Ni, Pt) nanoparticles having fcc cubo-octahedral geometry with 201, 586, 1289 and 2406 atoms. The results are compared with the known experimental results. Importance of the results in studying reactions on supported bimetallic catalysts has been highlighted.

PACS Codes: 68.35Bs, 68.35Md, 68.10Jy, 61.66Dk

\*Author for correspondence

Tel.: (91) (33) 337 5345

FAX: (91) (33) 337 4637

e-mail: badal@cmp.saha.ernet.in

## I. INTRODUCTION

Supported bimetallic catalysts are of enormous importance in petroleum and other chemical industries.<sup>1-3</sup> They are used for better selectivity of products in parallel reactions. Mostly, these bimetallic catalysts are supported nanostructures, which may have specific active sites like the corner sites, edge sites or sites on regular crystalline faces. In order to understand the catalytic activity and selectivity of a bimetallic nanostructure it is important to know the average surface composition and particularly the occupancy of various sites by A or B metal atoms of the A-B bimetallic system. Since in catalytic reactions the bimetallic catalyst surfaces are partially or totally covered by reacting gases, it is also important to study the surface composition in presence of reacting gases. It is the aim of the present work to study the spatial distribution of atoms for a few Pd-based bimetallic nanoparticles like Pd-Ag, Pd-Cu, Pd-Ni and Pd-Pt nanoparticles having dispersion in the range of 0.6 - 0.3 (the total number of atoms per particle being in the range of 200 - 2500). The motivation to study Pd-based systems follows from the fact that Pd is a very good catalyst for hydrogenation and oxidation reactions. Amongst the alloy systems, Pd-Pt catalysts are of great technological interest because of their use in (de)hydrogenation reactions, oxidation reaction, (dehydro)cyclization reaction, hydrogen peroxide production etc,<sup>4-8</sup> besides their use in electrochemical studies.<sup>9-10</sup> These catalysts have the additional advantage of being more resistant to poisoning by sulfur and nitrogen compounds than the respective monometallic catalysts.<sup>11</sup> Alloying Pd with copper and silver (Pd-Cu, and Pd-Ag systems) is found to greatly enhance the selectivity of Pd in the partial hydrogenation of dienes<sup>12</sup> and in the hydro-dehalogenation of olefinic compounds.<sup>13</sup> In these systems the Pd surface has to be partly covered by the second metal (Cu or Ag) in a carefully controlled way. This is achieved in bimetallic nanostructures. Besides, Pd-Cu systems show some promise as catalysts for simultaneous oxidation of CO and reduction of NO,<sup>14-15</sup>

the very vital reactions for automotive pollution control. Pd-Ni systems also show interesting features in their use as catalysts for 1,3-butadiene hydrogenation reaction. The Pd<sub>5</sub>Ni<sub>95</sub> system, for example, is found to have greater activity than the pure metals.<sup>16</sup> In view of the above interesting features we study in this work the atomic distribution in the above four Pd-based nanostructures in presence of different coverage ( $0 \leq \theta \leq 1$ ) of some simple adsorbates like hydrogen, oxygen, carbon monoxide (CO) and nitric oxide (NO). The plan of the paper is as follows: In section II we describe the formulation of the model. In section III we apply the formalism to the four Pd-based bimetallic nanoparticle system mentioned above. Conclusions are drawn in section IV.

## II. FORMULATION OF THE MODEL

The model used in this work is based on the Monte-Carlo (MC) simulation procedure adopted by Strohl and King<sup>17</sup> to study the segregation behavior of Pt-Ib bimetallic nanoparticles. However, we have introduced two modifications to their procedure as discussed below:

First, the pair bond energy required for MC simulation are evaluated taking into account the fact that the pair bond energies are dependent on the coordination number of the atoms. Thus, the pair bond energy between two nearest neighbor atoms,  $E_{ij}$ , is related to the site energy (or the partial bond energy)  $E_c^i(n)$  etc. as<sup>17</sup>

$$E_{ij} = w_{ij}/Z + E_c^i(n)/n + E_c^j(m)/m \quad (1)$$

where  $i, j = A$  or  $B$  atom of the general  $A_X B_{X-1}$  alloy and  $w_{ij} = 0$  if  $i = j$ .  $E_c^i(n)$  is the partial bond energy of the  $i$ -atom with  $n$  nearest neighbors etc.  $w_{ij}$  is the interchange energy for two dissimilar atoms which may be estimated from the excess heat of mixing; and  $Z$  is the bulk coordination number. In order to find  $E_c^i(n)$  Strohl and King used an empirical formula

$$E_c^i(n) = a^i + b^i n + c^i n^2 \quad (2)$$

where  $a^i$ ,  $b^i$  and  $c^i$  are constants for the  $i$ -metal and may be obtained from the experimental values of the heat of sublimation, the energy of bulk vacancy formation and the surface energy for (100) surface.

We use the  $a$ ,  $b$  and  $c$  values evaluated by Rousset et al.<sup>18</sup> from a modified tight binding method (MTB). Here, the parameters are determined from the experimental values of dimer energy, surface energy and the energy for monovacancy creation. In this MTB scheme the site energy for six-coordinated corner atom and the seven-coordinated edge atoms can be obtained from interpolation rather than extrapolation as was obtained in the work of Strohl and King. Once the site energies are known, the pair bond energies can be easily evaluated.<sup>19</sup> The second modification is made to consider the chemisorption. For the present study we have introduced necessary changes in the MC simulation to take into account the effect of chemisorption. Here we take an additional term  $\theta(E_A-E_B)$  in the configuration energy where  $\theta$  is the adsorbate coverage and  $E_{A(B)}$  is the chemisorption energy of the adsorbate on  $A(B)$  metal.<sup>20-21</sup> Once the constants  $a^i$ ,  $b^i$  and  $c^i$  are derived and the parameters  $w_{ij}/Z$ ,  $\theta$  and  $(E_A-E_B)$  are provided, the MC simulation is carried out in the usual manner until the equilibrium configuration energy is found. In essence, the atomic distribution results obtained in our nanostructure work would complement the segregation results obtained earlier by Rousset et al.<sup>18</sup> for the semi-infinite Pd-X alloy systems. In addition, the present results consider the role of various degrees of coverage of adsorbates on the atomic distribution.

### III. APPLICATIONS

In view of the fact that all the constituent metals of the bimetallic systems considered in this work have fcc structure, the particles with number of atoms in the range of 200 - 2500 may be assumed to have the fcc cubo-octahedral geometry. With this assumption we perform the MC simulation. The important input parameters used in the work are presented in Tables 1 and 2. In this simulation program the

important variable parameters are (a) the bimetallic system, (b) the bulk composition, (c) the adsorbate coverage, and (d) the temperature. Since the composition variation with temperature is well-known, we have performed the simulation for a typical alloy equilibration temperature (700K). Though we have performed simulation for several bulk compositions (20% Pd, 50% Pd, 66% Pd, 80% Pd), for convenience of comparison of several systems in presence of different adsorbates with varying coverage we would present results mostly for  $\text{Pd}_{50}\text{X}_{50}$  composition. The simulation results being very exhaustive cannot all be presented in this paper. We would be presenting some typical results of the systems. Readers interested in the details for other compositions, particle sizes, coverage or adsorbates may kindly contact the authors.

#### **A. Average surface Pd concentration**

In figure 1(a) we have plotted for the  $\text{Pd}_{50}\text{Ag}_{50}$  nanosystem the fraction of surface sites occupied by Pd atoms for different particle size and H coverage. In Figs. 1(b), (c) and (d) similar results are plotted for the oxygen, CO and NO adsorption. Several characteristics are to be noted:

- (i) For clean  $\text{Pd}_{50}\text{Ag}_{50}$  nanoparticles of all sizes Ag segregates to the surface sites.
- (ii) As the coverage increases the fraction of Pd surface atom increases leading to a reduction in Ag segregation and ultimately Pd atoms tend to segregate to the surface sites.

This is true for all particle sizes and all the four adsorbates under consideration. In case of CO adsorbate Pd atoms seem to segregate to the surface sites even at coverage 0.25, while for other gases the segregation reversal takes place at coverage close to one. This behavior can be interpreted as a result of the higher heat of adsorption of adsorbates on Pd compared to that on Ag. Higher binding energy of adsorbates causes Pd atoms to move to the surface countering the normal segregat-

ing force. The difference in heat of CO adsorption on Pd and Ag being very large ( $\approx 28$  kcal/mole), Pd atoms start segregating to the surface even at low coverage. It may be noticed that for clean and small coverage of adsorbates the Ag surface fraction increases as the particle size increases (smaller dispersion). This follows from the fact that the fraction of surface sites decreases with increase in particle size; and therefore, the Ag atoms, if available, can cover higher fraction of surface sites for clean and small coverage (please see Table 4 of Strohl and King<sup>17</sup>). However, as the coverage increases, more Pd atoms move to the surface due to stronger binding to the adsorbate; and thus, the Pd surface fraction increases with increase in particle size.

Figs. 2(a)-(d) show the Pd surface fraction for the Pd<sub>50</sub>Cu<sub>50</sub> nanoparticles in presence of the adsorbed gases. For this bimetallic system, Cu segregates to the surface for hydrogen coverage up to 0.6 for larger particles. For smaller particles Cu segregates for hydrogen coverage even up to 0.75. For still larger coverage Pd segregates to the surface. For oxygen as adsorbates on Pd<sub>50</sub>Cu<sub>50</sub> system, Cu segregates for all coverages and all particle sizes studied in this work. Higher the coverage, higher is the extent of Cu segregation. This again follows from the heat of adsorption difference criterion mentioned before. Here binding energy of oxygen on copper is higher than that on Pd. For CO and NO adsorption on the Pd<sub>50</sub>Cu<sub>50</sub> nanoparticles Cu segregates for clean and very low coverage. For CO and NO coverage  $>0.25$  the Pd atoms start segregating to the surface.

The difference in the heat of adsorption of hydrogen (oxygen) on pure Pd and Ni metals is very small. This causes only small changes in the surface Pd concentration with coverage for the Pd<sub>50</sub>Ni<sub>50</sub> system (Figs. 3(a) and (b)). For all particle sizes and coverage up to one Ni segregates to the surface. For CO and NO adsorption on Pd<sub>50</sub>Ni<sub>50</sub>, on the other hand, Pd atoms start segregating to the surface from coverage 0.2 (please see Figs. 3(c) and (d)). The segregation behavior of the

$\text{Pd}_{50}\text{Pt}_{50}$  system is very simple. The clean system shows Pd segregation. And for all particle sizes and all adsorbates Pd surface concentration slowly increases with increase in coverage (please see Figs. 4(a)-(d)).

In order to compare the segregation behavior of the bimetallic  $\text{Pd}_{50}\text{X}_{50}$  nanosystems in presence of different adsorbates we plot in figure 5(a)-(d) the Pd surface fraction for a particular coverage,  $\theta = 0.5$ . It may be noticed that in presence of hydrogen or oxygen (Figs. 5(a) and (b) respectively) Pd segregates to the surface sites only for the Pd-Pt system. For the rest of the systems the other component segregates. In presence of CO, however, Pd segregates for all systems and for all particle sizes (Fig. 5(c)). In presence of NO, only for the Pd-Ag system Ag segregates, while for the rest of the systems Pd segregates to the surface sites (Fig.5(d)). The role of adsorbate coverage on the surface Pd concentration for the different bimetallic systems has been shown in Figs. 6(a)-(d) for the four different adsorbates. The results are for particles having 586 atoms (dispersion  $D = 0.457$ ). The figures are self-explanatory. Except for hydrogen on  $\text{Pd}_{50}\text{Ni}_{50}$  (Fig. 6(a)) and oxygen on  $\text{Pd}_{50}\text{Ni}_{50}$  and  $\text{Pd}_{50}\text{Cu}_{50}$  (Fig. 6 (b)) for all other systems Pd surface fraction increases with coverage.

## **B. Site occupancy and surface coordination**

Besides the overall surface Pd concentration for Pd-X nanoparticles it is also very important to know the occupancy of various types of surface sites on the fcc cubooctahedron particle. On the particle surfaces there are 6-coordinated corner sites, 7-coordinated edge sites, 8-coordinated fcc(100)-like face sites and 9-coordinated fcc(111)-like face sites. In figures 7(a)-(d) we have shown how for CO adsorption on 586-atom nanoparticles of the four bimetallic systems the fraction of Pd atoms on the 6, 7, 8 and 9-coordinated surface sites changes with coverage. For CO on  $\text{Pd}_{50}\text{Ag}_{50}$  system (Fig. 7(a)) at low coverage the 6 and 7 -coordinated sites are generally occupied by Ag atoms. As the coverage increases, gradually all types of

sites get increasingly occupied by Pd atoms. And at full monolayer coverage except the 8 -coordinated sites all other sites are occupied by Pd atoms. This is also the case for Pd<sub>50</sub>Cu<sub>50</sub> (Fig. 7(b)) system. In case of Pd<sub>50</sub>Ni<sub>50</sub> system (Fig. 7(c)) no particular type of surface sites is occupied fully by Pd or Ni atoms at any of the coverage from zero to one. In case of Pd<sub>50</sub>Pt<sub>50</sub> system the occupancy of the 9-coordinated sites changes very slowly from 0.72 to 0.78 as the coverage increases from zero to one. For NO adsorption the coverage-dependent site occupancy results for the four bimetallic systems are shown in figures 8(a) to (d). The results are self-explanatory.

For studying the relative occupancy of various sites in the four bimetallic systems we plot in figures 9(a)-(b) the site occupancy in the systems for a particular coverage ( $\theta$ ) and a particular particle size (586-atom nanoparticles). The adsorbates considered are CO and NO. For both the adsorbates, it may be noticed that at this 0.5 coverage the 6-coordinated sites are almost fully occupied by Pd in case of Pd<sub>50</sub>Pt<sub>50</sub> system. On the other hand, for the Pd<sub>50</sub>Ag<sub>50</sub> and Pd<sub>50</sub>Cu<sub>50</sub> systems the 6 -coordinated sites are generally occupied by Ag and Cu atoms respectively.

### **C. Size dependence of surface site occupancy**

Particle size, quite often, plays an important role in catalysis. In bimetallic systems, this has an additional significance. Because, different metallic atoms may preferentially occupy different type of sites. In order to study this aspect we show in figure 10(a)-(d) how for a CO coverage of 0.5 the surface sites of a 586-atom nanoparticle are preferentially occupied by one type of atom or the other. What we find is that there is no general rule for occupancy of various sites as the particle size increases as there are crossovers of curves for different particle sizes in each of the four systems. In case of Pd<sub>50</sub>Ag<sub>50</sub> system (Fig. 10(a)) the occupancy of 8 and 9-coordinated sites by Pd atoms does not change much with particle size. But there are fluctuations in the occupancy of 6 and 7-coordinated sites by Pd atoms as the



particle size increases. Similarly, in case of Pd<sub>50</sub>Cu<sub>50</sub> and Pd<sub>50</sub>Ni<sub>50</sub> system there are fluctuations in occupancy of all types of surface sites as the particle size increases (Figs. 10(b) and (c)). In case of Pd<sub>50</sub>Pt<sub>50</sub> we find some systematic variation in the occupancy of various surface sites. As the number of atoms in the particle increases from 201 to 2406, the occupancy of 9-coordinated sites by Pd atoms increases significantly. This variation is distinctively different from other bimetallic systems.

The net result of the model presented in this work is that we have simulated the probable surface composition and the atomic distribution for the nanoparticles of some Pd-based bimetallics in presence of various coverages of simple gases like hydrogen, oxygen, CO and NO. However, the experimental results are scarce, particularly for adsorbed systems. In the zero-coverage limit, i.e. for clean bimetallic nanoparticles experimental results exist for the PdPt and PdCu systems. The model shows Pd segregation for the PdPt system and Cu segregation for the Pd-Cu system in agreement with the experimental results.<sup>19,26</sup> But the coverage-dependent surface composition and site occupancy are yet to be experimentally realized. However, in the absence of experimental results, the present model can serve some purpose in estimating the probable surface composition for the nanoparticles under various coverage of gases. Besides, the knowledge of the site occupancy by A type atom or by B type atom of A-B bimetallic atoms may sometime help to identify the active sites on a catalyst for a particular catalytic reaction. For example, it has been found that the rate of 1,3-butadiene hydrogenation reaction on a Pd<sub>5</sub>Ni<sub>95</sub> system is larger than that on pure metals.<sup>16</sup> This may be due to the ensemble effect whereby a particular form of ensemble of Pd and Ni atoms form the active site. Such behavior may be explained from a knowledge of the site occupancy as studied in this work.<sup>27</sup>

#### IV. CONCLUSIONS

Monte-carlo simulations are carried out to find out the nature of occupancy of surface sites of Pd-based bimetallic nanoparticles. We upgraded the earlier MC

simulation scheme of Strohl and King<sup>17</sup> with input data obtained from improved cohesive energy calculation.<sup>18</sup>

- (a) It has shown how the overall surface composition varies with particle size, the nature of adsorbed gas and its coverage .
- (b) It has also been shown how for a particular adsorbed gas the surface composition varies from one bimetallic system to the other.
- (c) We have also shown how different types of surface sites of the bimetallic systems are occupied and how the occupancy of these sites varies with gas coverage.
- (d) We have discussed briefly the importance of such studies in understanding the role of active sites in catalysis.

The validity of the model would be justified after more and more experimental data and particularly for gas-covered surfaces, are available.

#### **ACKNOWLEDGMENTS:**

Mahesh Menon thanks the Council of Scientific and Industrial Research, New Delhi, for the award of a Senior Research Fellowship (No. 9/420/(12)/95-EMR-I) to carry out this work. BCK acknowledges receipt of the basic MC program for segregation studies from Prof. Terry King.

#### **REFERENCES**

1. J. H. Sinfelt, *Bimetallic Catalysts* (Wiley, New York, 1983).
2. V. Ponec, *Adv. Catal.* **32**, 149 (1983).
3. V. Ponec, *Catal. Rev. Sci. Eng.* **18**, 151 (1978).

4. L. C. A. Van den Oetelaar, O. W. Nooij, S. Oerlemans, A. W. Denier van der Gon, H. H. Brongersma, L. Lefferts, A. G. Roosenbrand, and J. A. R. Van Veen, *J. Phys. Chem.* **B 102**, 3445 (1998).
5. D. W. McKee, and P. J. Norton, *J. Catal.* **3**, 252 (1964).
6. Y. Deng, and L. An, *Appl. Catal.* **A 119**, 13 (1994).
7. S. Vigneron, P. Deprelle, and J. Hermia, *Catal. Today* **27**, 229 (1996).
8. T. Koscielski, Z. Karpinski, and Z. Paal, *J. Catal.* **77**, 539 (1982).
9. K. V. Ramesh, P. R. Sarode, S. Vasudevan, and A. K. Shukla, *J. Electroanal. Chem* **223**, 91 (1987).
10. G. A. Attard, and R. Price, *Surf. Sci.* **335**, 63 (1995).
11. T. B. Lin, C. A. Jan, and J. R. Chang, *Ind. Eng. Chem. Res.* **34**, 4284 (1995).
12. J. Philips, A. Auroux, G. Bergeret, J. Massardier, and A. Renouprez, *J. Phys. Chem.* **97**, 3565 (1993).
13. E. N. Balko, E. Przybylski, and F. Von Trentini, *Appl. Catal.* **B2**, 1 (1993).
14. Y. Debauge, P. Ruiz, J. Massardier, M. Abon, and J. C. Bertolini, *Proceedings of 3<sup>rd</sup> International Conference on Combustion Technologies for a clean environment (Lisbon, Portugal, 1995) Vol. 2, Paper No. 29.1.*
15. Y. Debauge, M. Abon, J. C. Bertolini, J. Massardier, and A. Rochefort, *Appl. Surf. Sci.* **90**, 15 (1995).
16. P. Miegge, J. L. Rousset, B. Tardy, J. Massardier, and J. C. Bertolini, *J. Catal.* **149**, 404 (1994).
17. J. K. Strohl, and T. S. King, *J. Catal.* **116**, 540 (1989).

18. J. L. Rousset, J. C. Bertolini ,and P. Miegge, Phys. Rev. **B 53**, 4947 (1996).
19. J. L. Rousset, B. C. Khanra, A. M. Cadrot, F. Cadete Santos Aires, A. Renouprez, and M. Pellarin, Surf. Sci. **352-354**, 583 (1996).
20. T. S. King, and R. G. Donnelly, Surf. Sci. **141**, 417 (1984).
21. B. C. Khanra and M. Menon, Int. J. Mod. Phys. B (in press).
22. G. Ertl, in *The Nature of the Surface Chemical Bond*, edited by T. N. Rhodin and G. Ertl (North-Holland, Amsterdam, 1979) p.319.
23. E. Shustorovich, Surf. Sci. Rep. **6**, 1 (1986).
24. D. Tomanek, S. Mukherjee, V. Kumar, and K. H. Bennemann, Surf. Sci. **114**, 11 (1982).
25. J. L. Gland, B. A. Sexton, and G. Fisher, Surf. Sci. **95**, 587 (1980).
26. A. J. Renouprez, K. Lebas, G. Bergeret, J. L. Rousset, and P. Delichere, Studies in Surface Science and Catalysis **101**, 1105 (1996).
27. B. C. Khanra and M. Menon, Chem. Phys. Lett. (in Press)

## FIGURE CAPTIONS

- Fig. 1. MC simulated surface fraction of Pd atoms on bimetallic Pd<sub>50</sub>Ag<sub>50</sub> nanoparticles as a function of dispersion and coverage of various adsorbates: (a) Adsorbate: hydrogen; (b) Adsorbate: oxygen; (c) Adsorbate: CO; (d) Adsorbate: NO.
- Fig. 2. MC simulated surface fraction of Pd atoms on bimetallic Pd<sub>50</sub>Cu<sub>50</sub> nanoparticles as a function of dispersion and coverage of various adsorbates: (a) Adsorbate: hydrogen; (b) Adsorbate: oxygen; (c) Adsorbate: CO; (d) Adsorbate: NO.
- Fig. 3. MC simulated surface fraction of Pd atoms on bimetallic Pd<sub>50</sub>Ni<sub>50</sub> nanoparticles as a function of dispersion and coverage of various adsorbates: (a) Adsorbate: hydrogen; (b) Adsorbate: oxygen; (c) Adsorbate: CO; (d) Adsorbate: NO.
- Fig. 4. MC simulated surface fraction of Pd atoms on bimetallic Pd<sub>50</sub>Pt<sub>50</sub> nanoparticles as a function of dispersion and coverage of various adsorbates: (a) Adsorbate: hydrogen; (b) Adsorbate: oxygen; (c) Adsorbate: CO; (d) Adsorbate: NO.
- Fig. 5. MC simulated surface fraction of Pd atoms on bimetallic Pd<sub>50</sub>X<sub>50</sub> nanoparticles as a function of dispersion and 0.5 coverage of various adsorbates. (X = Ag, Cu, Ni, Pt). (a) Adsorbate: hydrogen; (b) Adsorbate: oxygen; (c) Adsorbate: CO; (d) Adsorbate: NO.
- Fig. 6. MC simulated surface fraction of Pd atoms on 586-atom bimetallic Pd<sub>50</sub>X<sub>50</sub> nanoparticles as a function of coverage of various adsorbates. (X = Ag, Cu, Ni, Pt). (a) Adsorbate: hydrogen; (b) Adsorbate: oxygen; (c) Adsorbate: CO; (d) Adsorbate: NO.

- Fig. 7. MC simulated surface fraction of Pd atoms at N-coordinated surface sites (N= 6-9) of a 586-atom Pd<sub>50</sub>X<sub>50</sub> nanoparticle in presence of various coverage of CO. (a) X= Ag; (b) X= Cu; (c) X=Ni; (d) X= Pt.
- Fig. 8. MC simulated surface fraction of Pd atoms at N-coordinated surface sites (N= 6-9) of a 586-atom Pd<sub>50</sub>X<sub>50</sub> nanoparticle in presence of various coverage of NO. (a) X= Ag; (b) X= Cu; (c) X=Ni; (d) X= Pt.
- Fig. 9. MC simulated surface fraction of Pd atoms at N-coordinated surface sites (N= 6-9) of a 586-atom Pd<sub>50</sub>X<sub>50</sub> nanoparticle (X = Ag, Cu, Ni, Pt) for 0.5 coverage of adsorbates. (a) Adsorbate: CO; (b) Adsorbate:NO.
- Fig. 10. MC simulated surface fraction of Pd atoms at N-coordinated surface sites (N= 6-9) of Pd<sub>50</sub>X<sub>50</sub> nanoparticle of different sizes in presence of 0.5 coverage of CO. (a) X= Ag; (b) X= Cu; (c) X= Ni; (d) X= Pt.

Table 1  
Input energy parameters for Pd-X bimetallic particles

system	$w_{Pd-X}$	$E_H$	$E_O$	$E_{CO}$	$E_{NO}$
Pd-X	(ev)	(kcal/mol)	(kcal/mol)	(kcal/mol)	(kcal/mol)
Cu	-0.0197	-56 <sup>a</sup>	-103 <sup>a</sup>	-12 <sup>a</sup>	-14 <sup>c</sup>
Ag	-0.00957	-56 <sup>a</sup>	-80 <sup>a</sup>	-6 <sup>a</sup>	-25 <sup>a</sup>
Ni	-0.0095	-63 <sup>a</sup>	-90 <sup>c</sup>	-27 <sup>a</sup>	-25 <sup>a</sup>
Pt	-0.00396	-61 <sup>b</sup>	-85 <sup>d</sup>	-32 <sup>a</sup>	-27 <sup>a</sup>
Pd	0	-62 <sup>a</sup>	-87 <sup>a</sup>	-34 <sup>a</sup>	-31 <sup>a</sup>

(a) Ref. 22, (b) Ref. 23, (c) Ref. 24, (d) Ref. 25, (e) Ref. 15

Table 2  
a, b, and c parameters for different metals

	Pd	Cu	Ag	Ni	Pt
a	-0.17702	-0.34040	-0.25866	-0.42578	-0.42874
b	-0.04842	-0.01177	-0.013283	-0.01447	-0.04750
c	0.00299	0.00129	0.00119	0.00160	0.00355

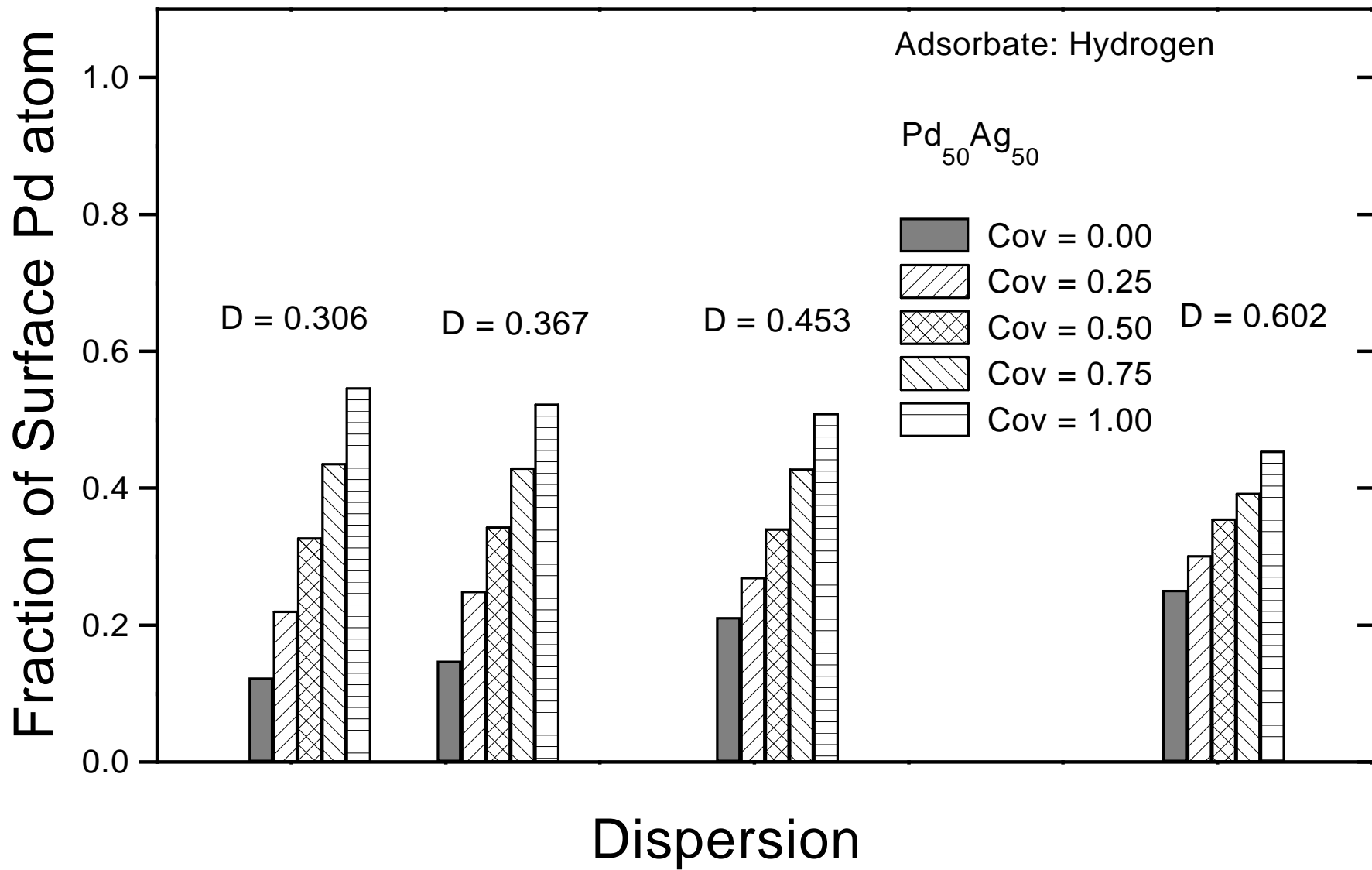


Fig. 1a  
 Menon + Khanra



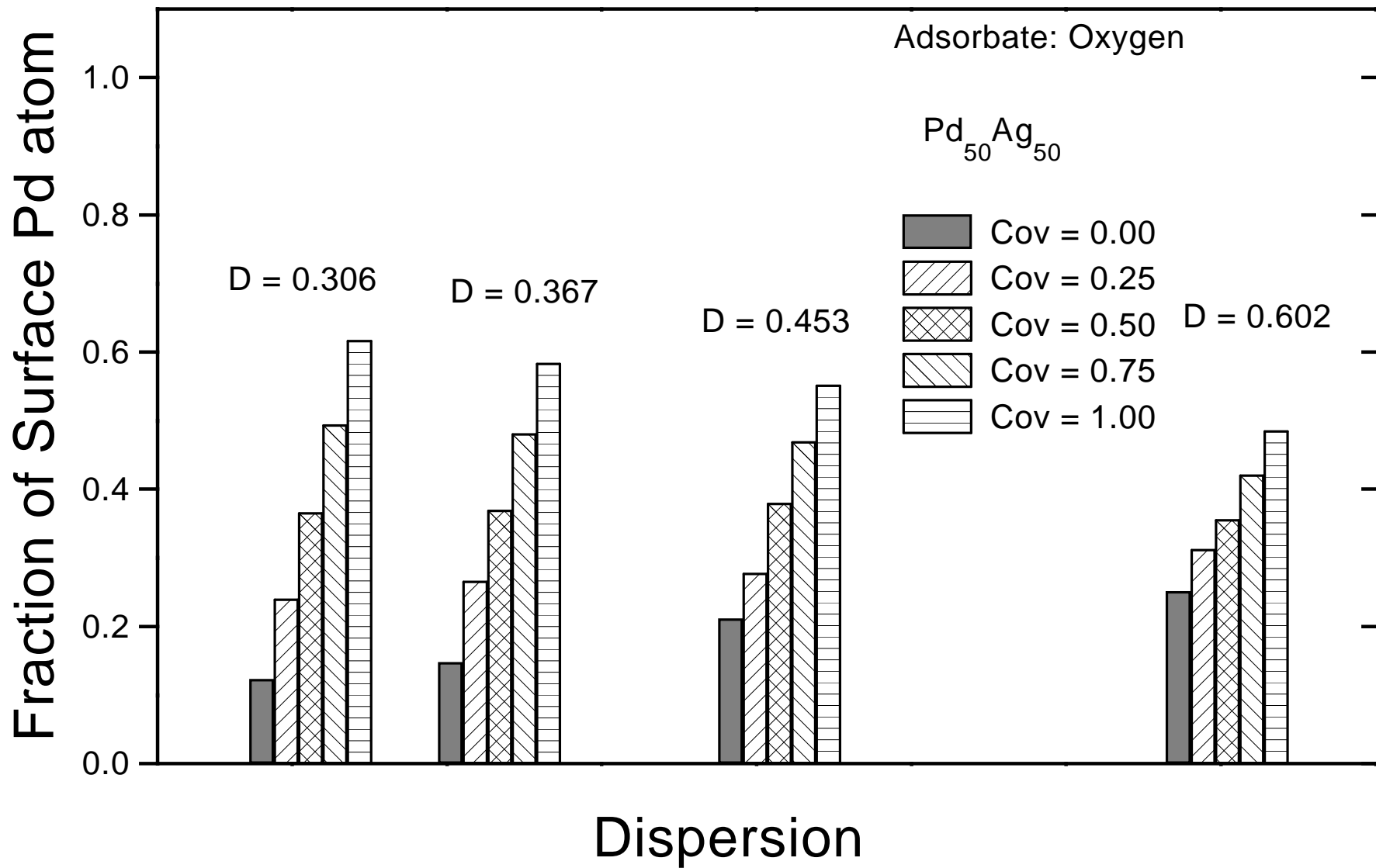


Fig. 1b  
Menon + Khanra

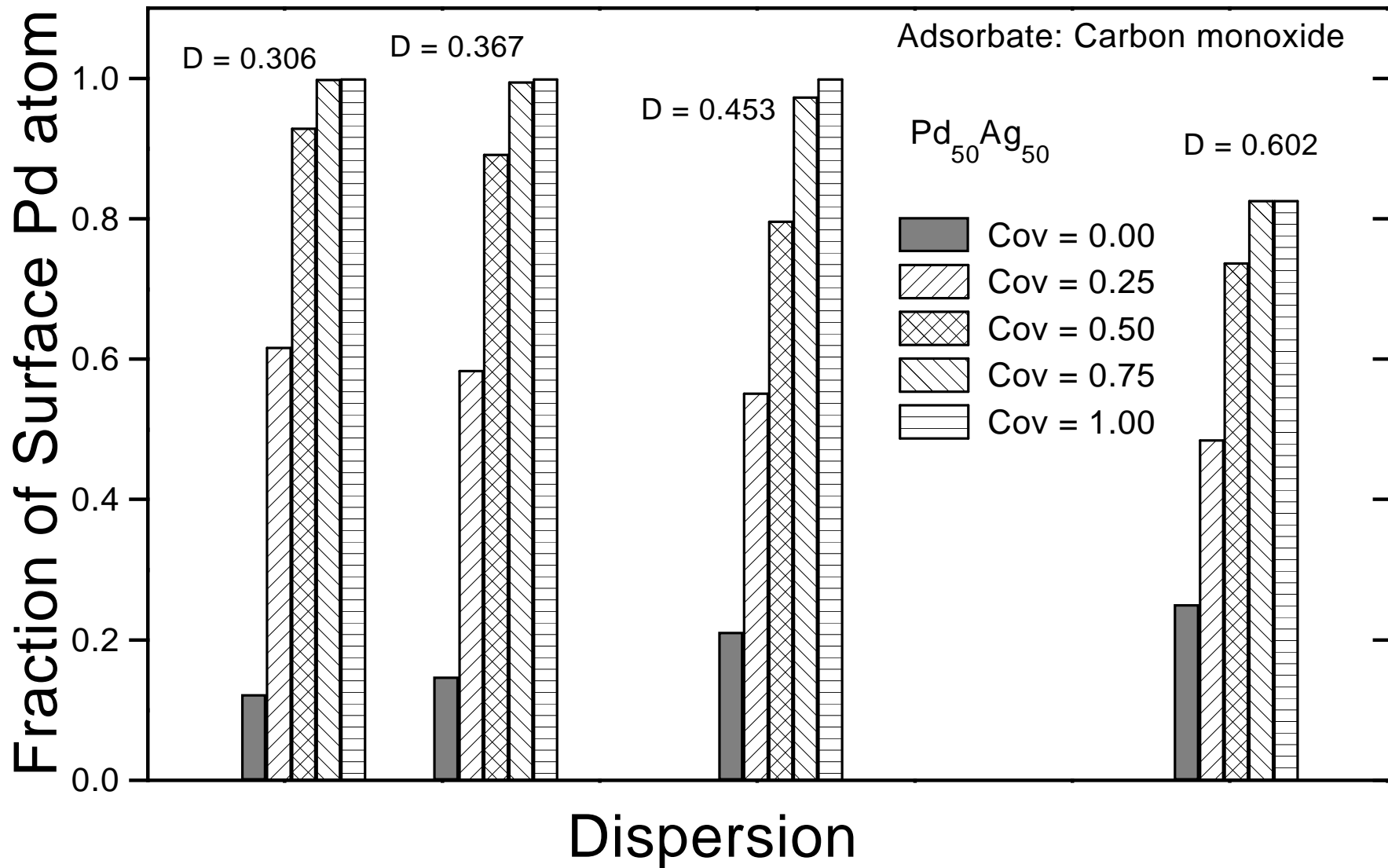


Fig. 1c  
Menon + Khanra

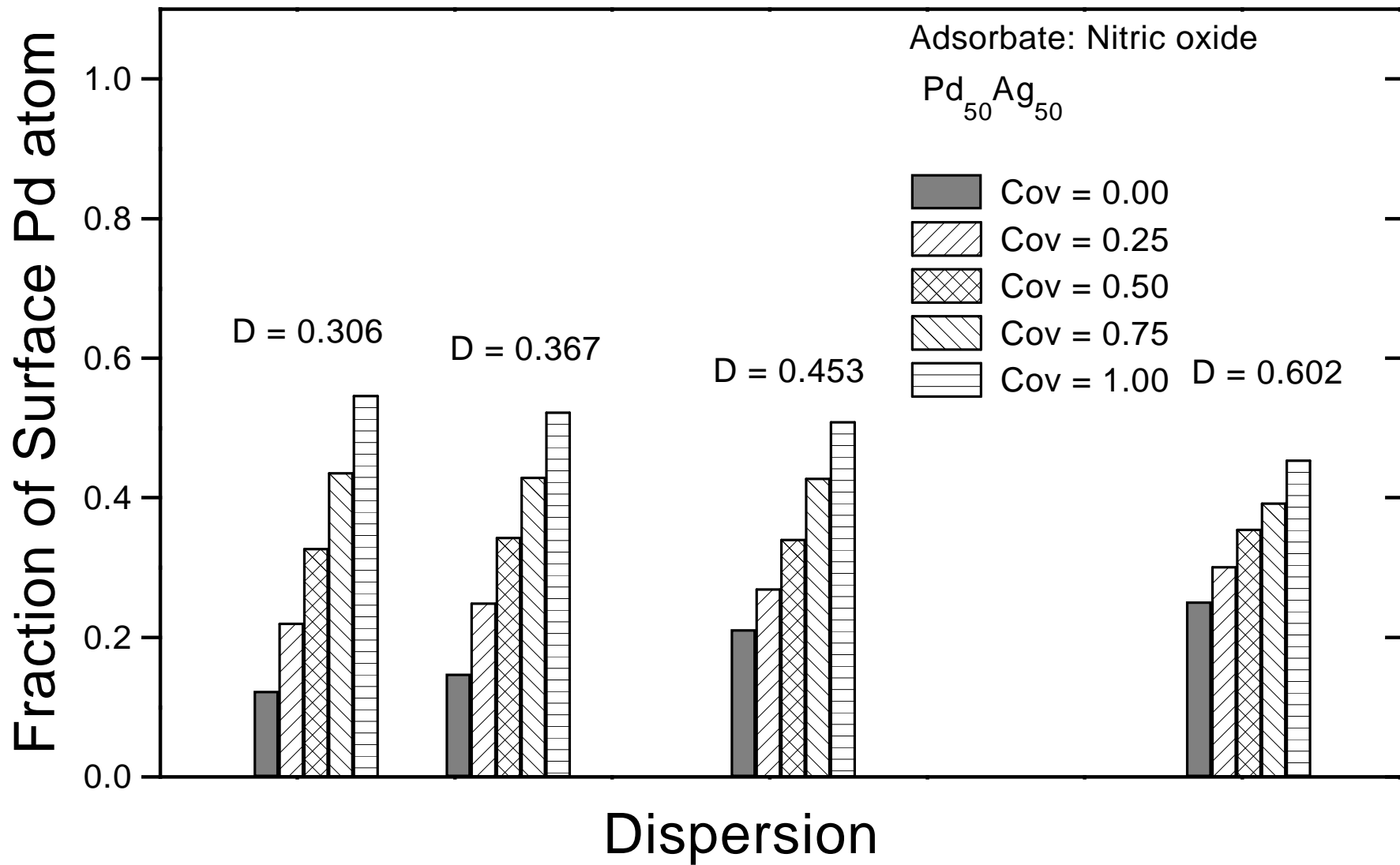


Fig. 1d  
Menon + Khanra

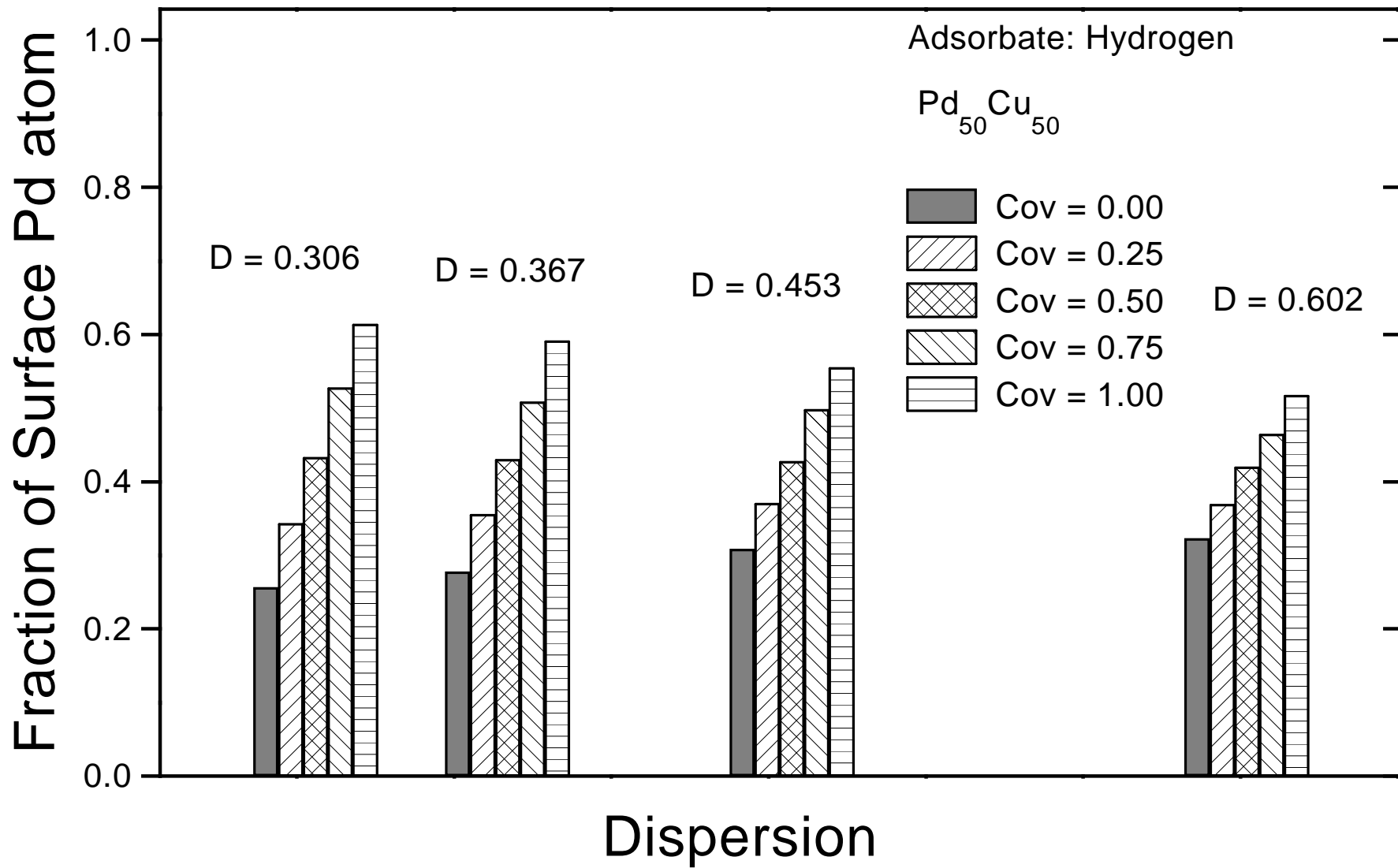


Fig. 2a  
Menon + Khanra

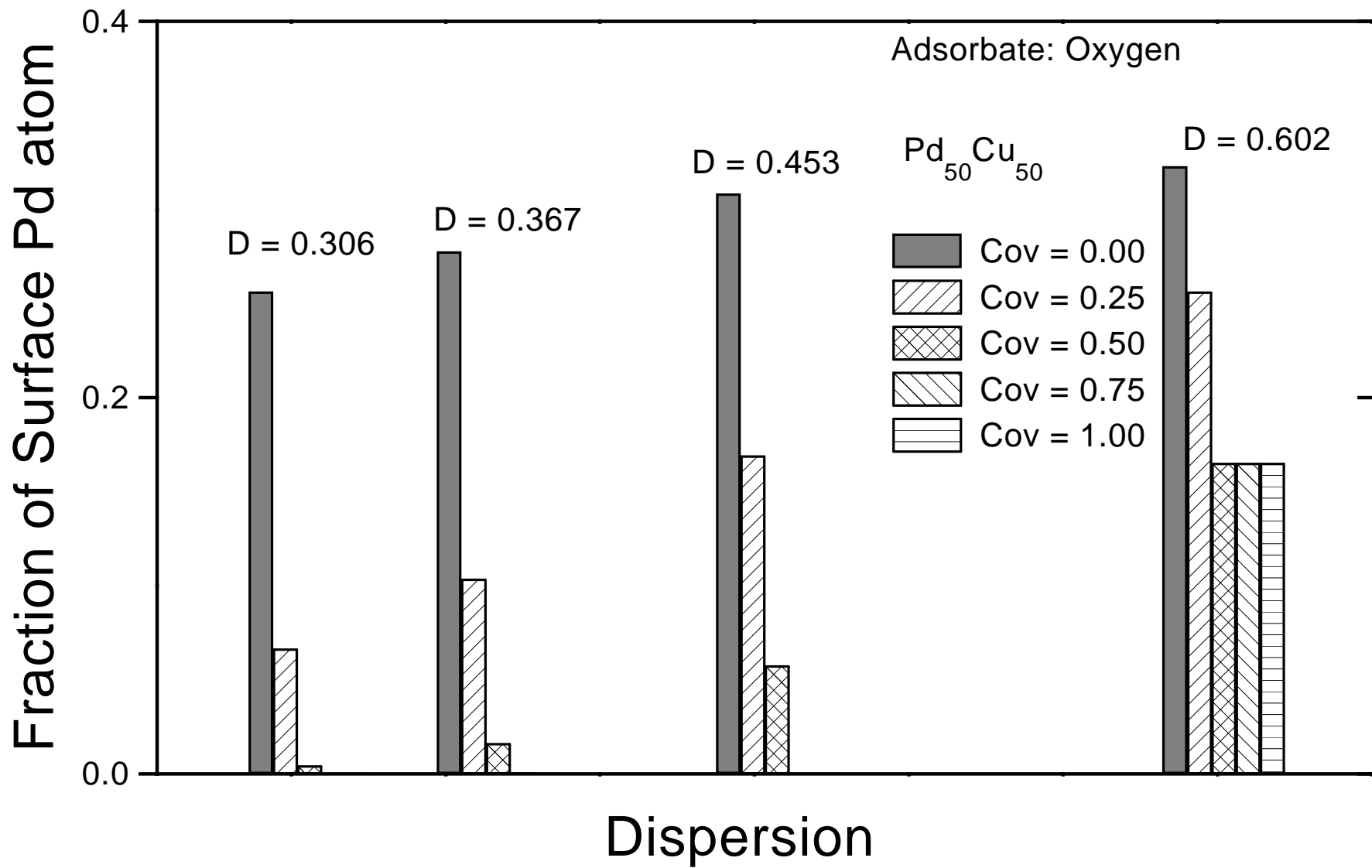


Fig. 2b  
Menon + Khanra

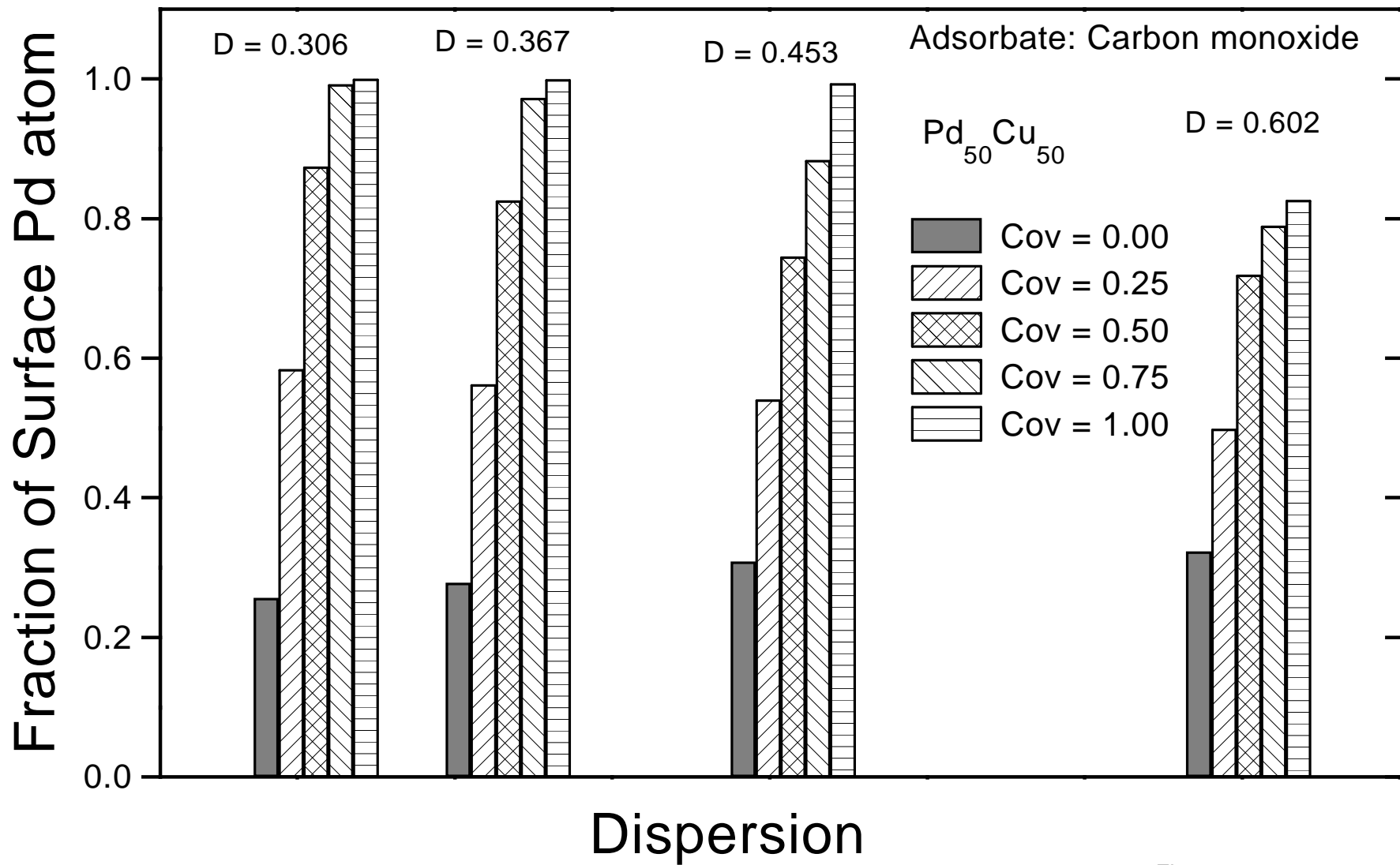


Fig. 2c  
Menon + Khanra

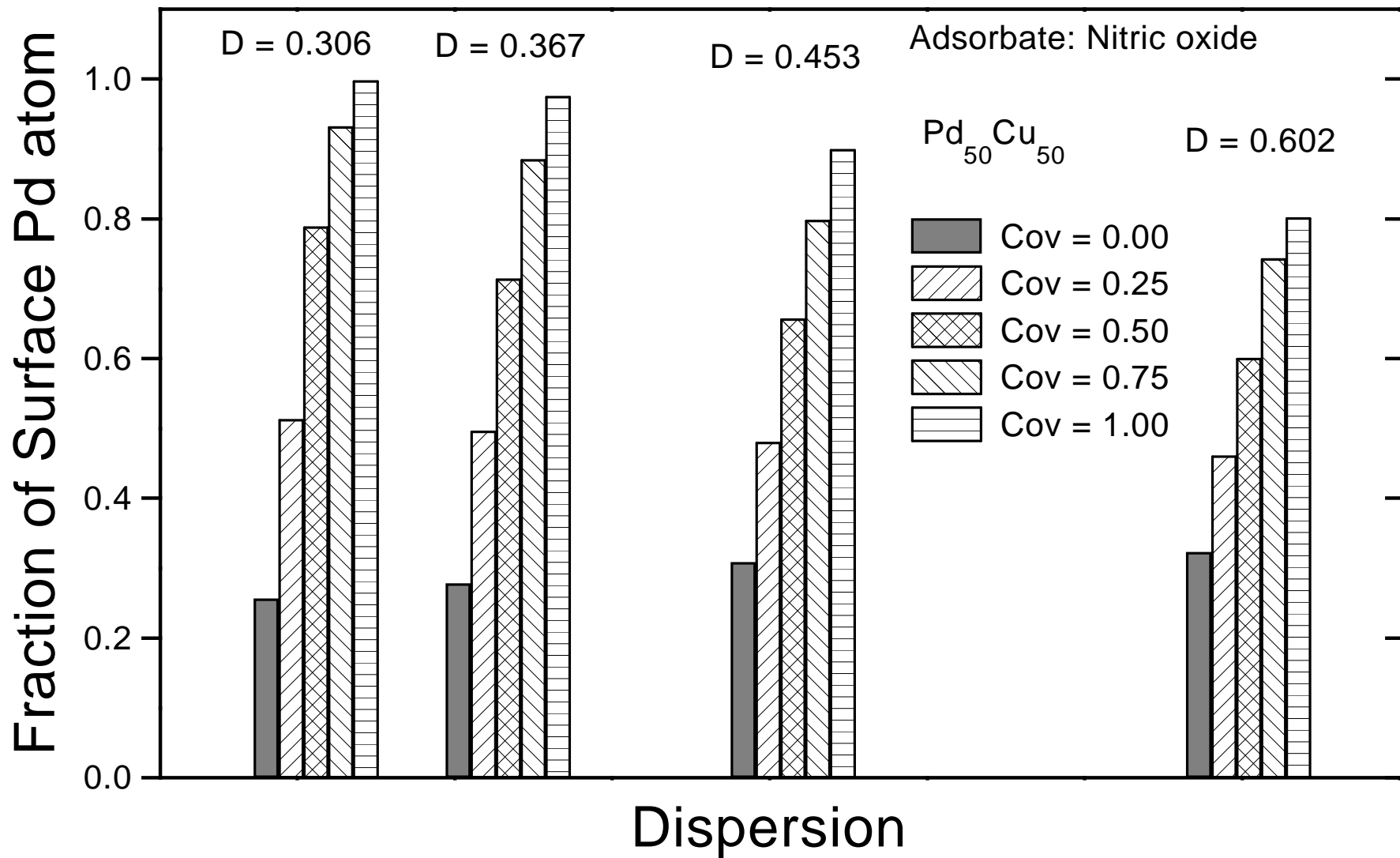


Fig. 2d  
Menon + Khanra

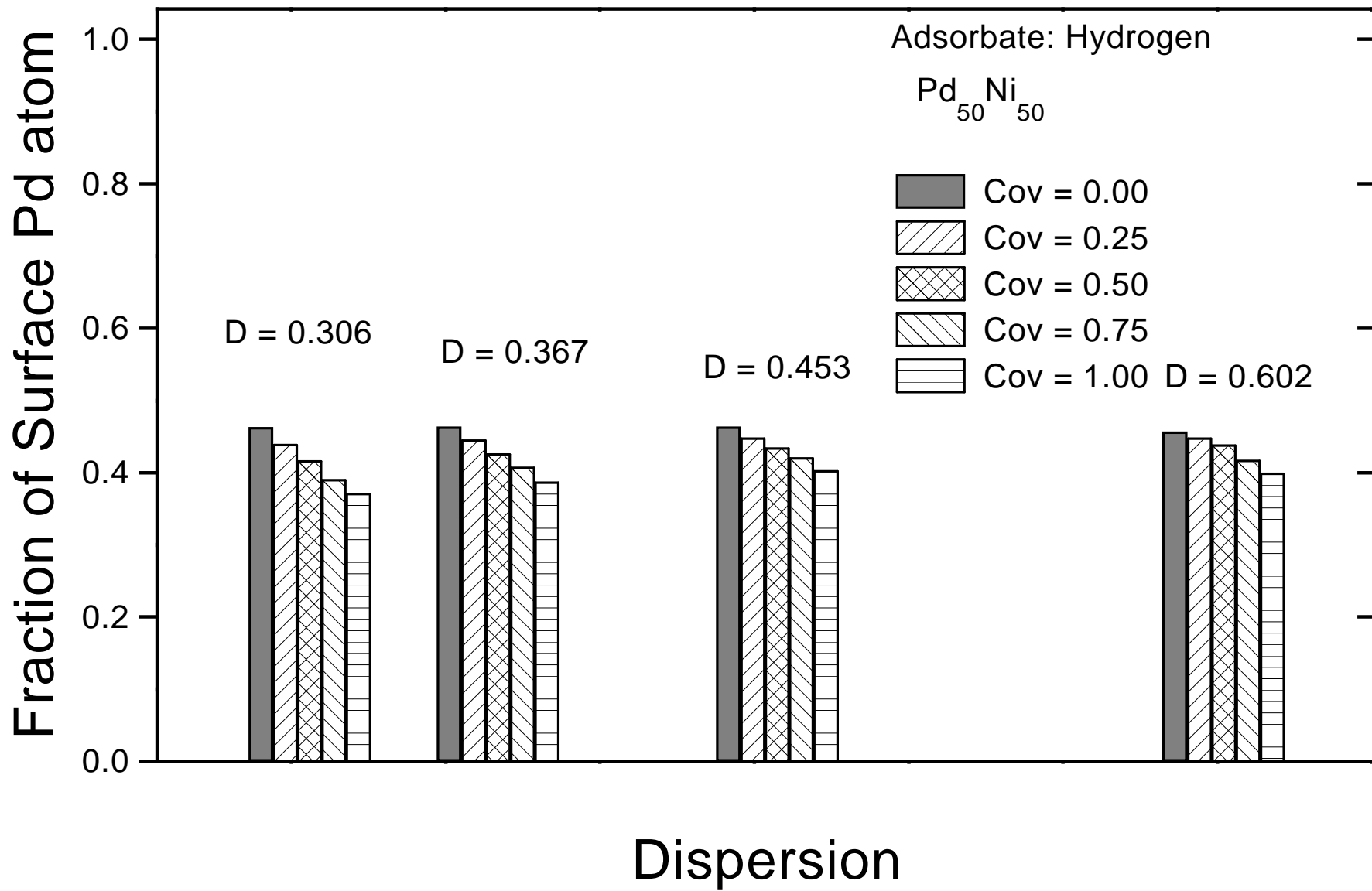


Fig. 3a  
Menon+ Khanra



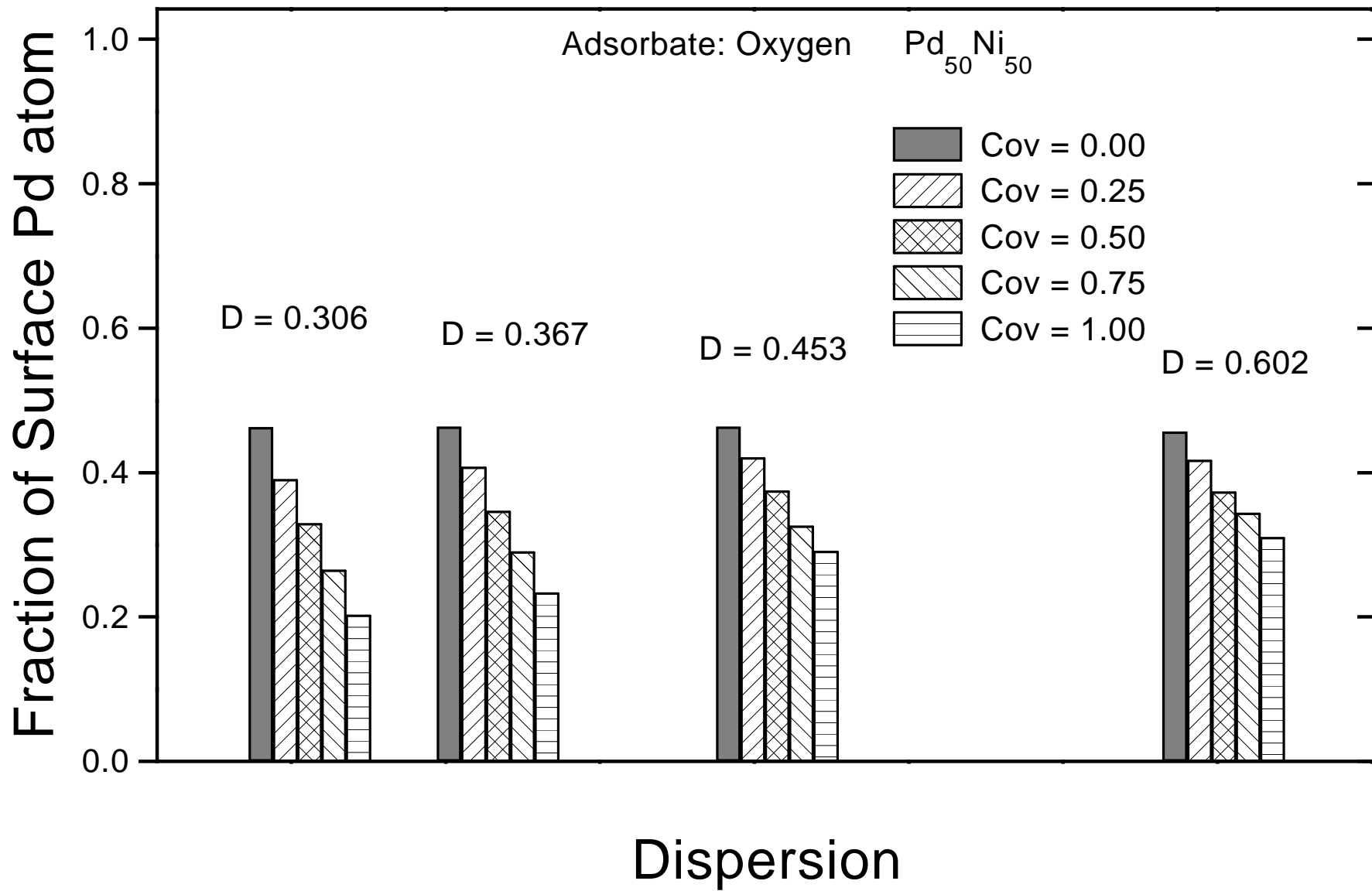


Fig. 3b  
Menon+Khanra

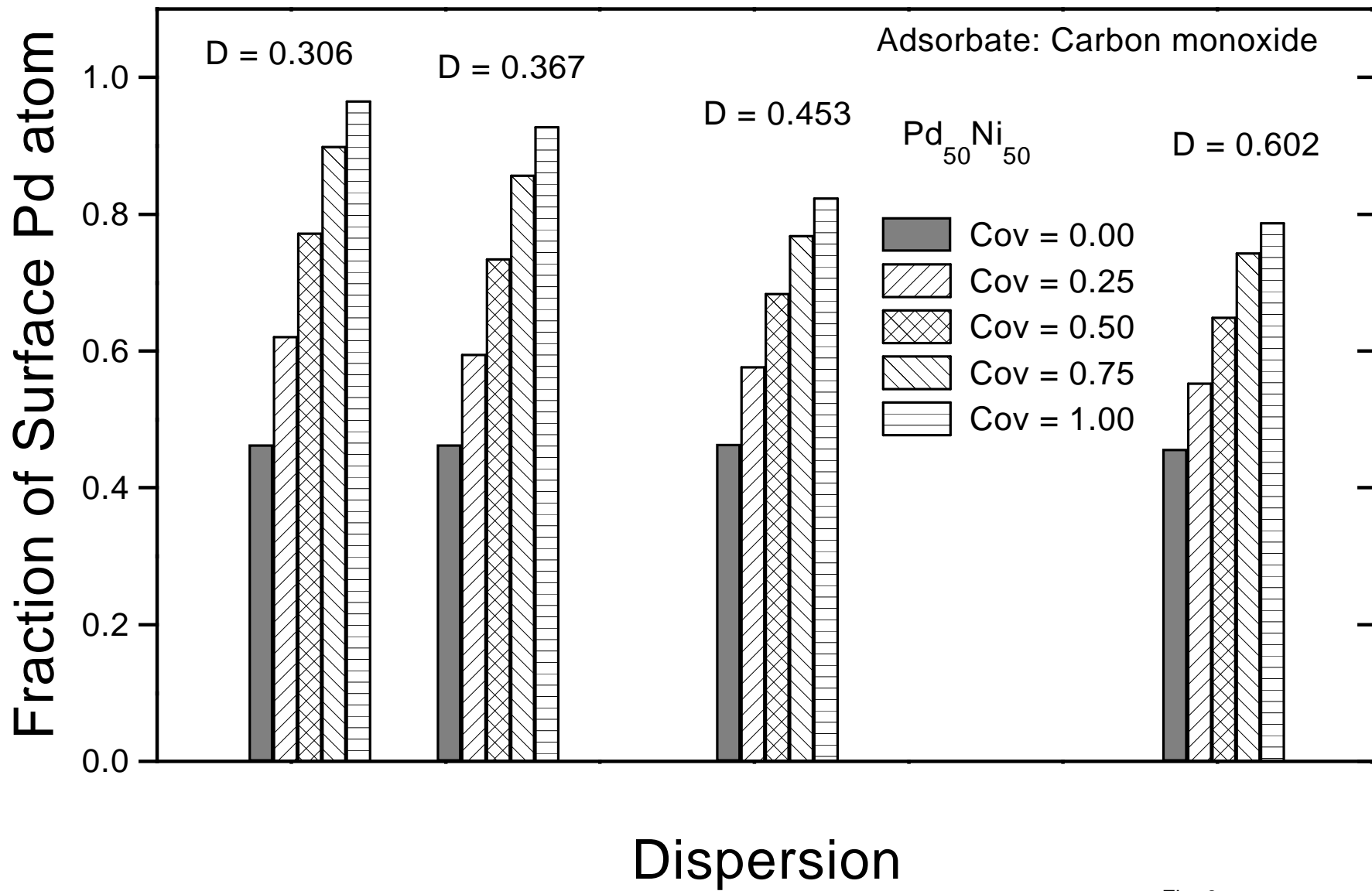


Fig. 3c  
Menon + Khanra

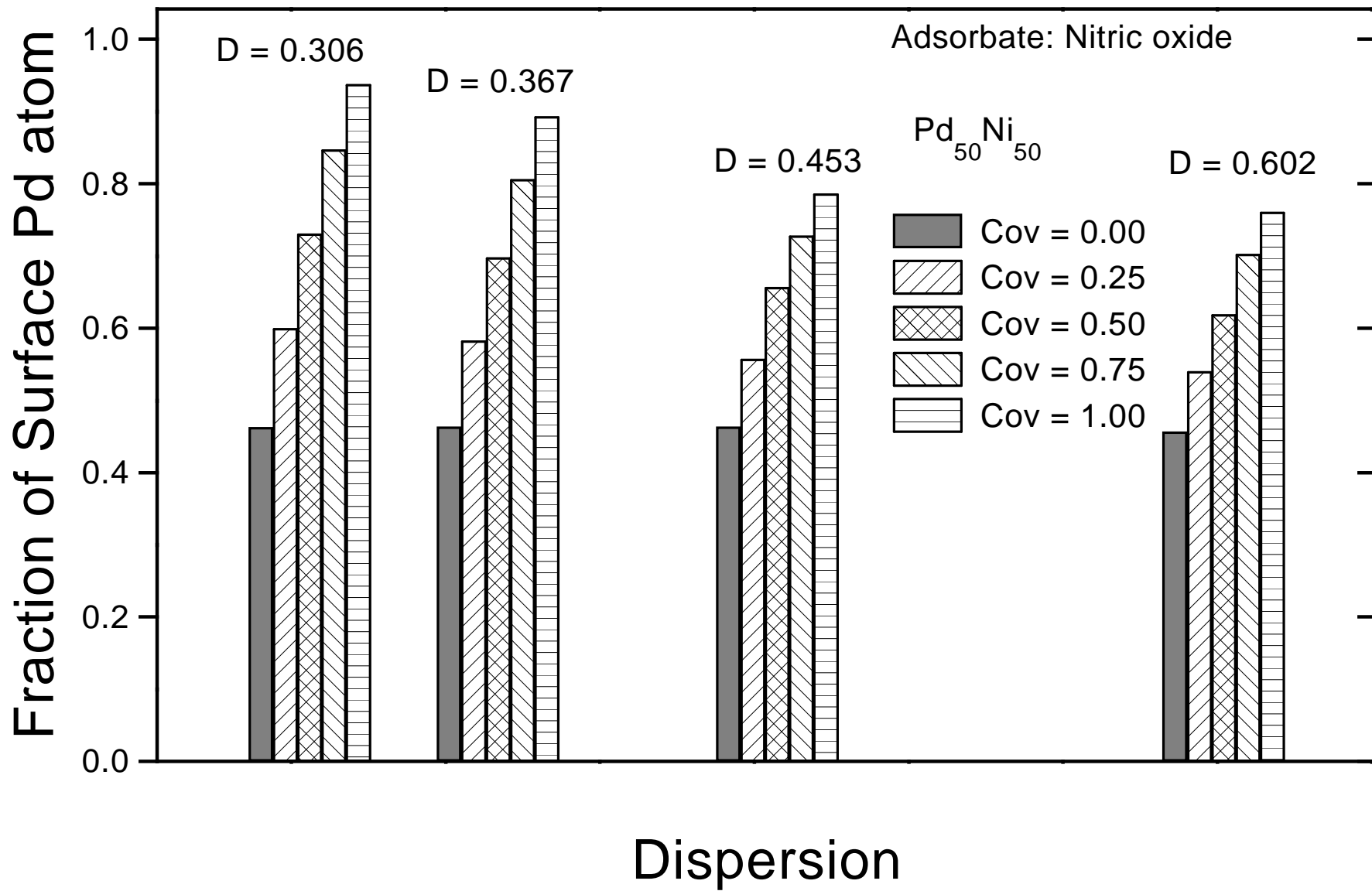


Fig. 3d  
 Menon + Khanra

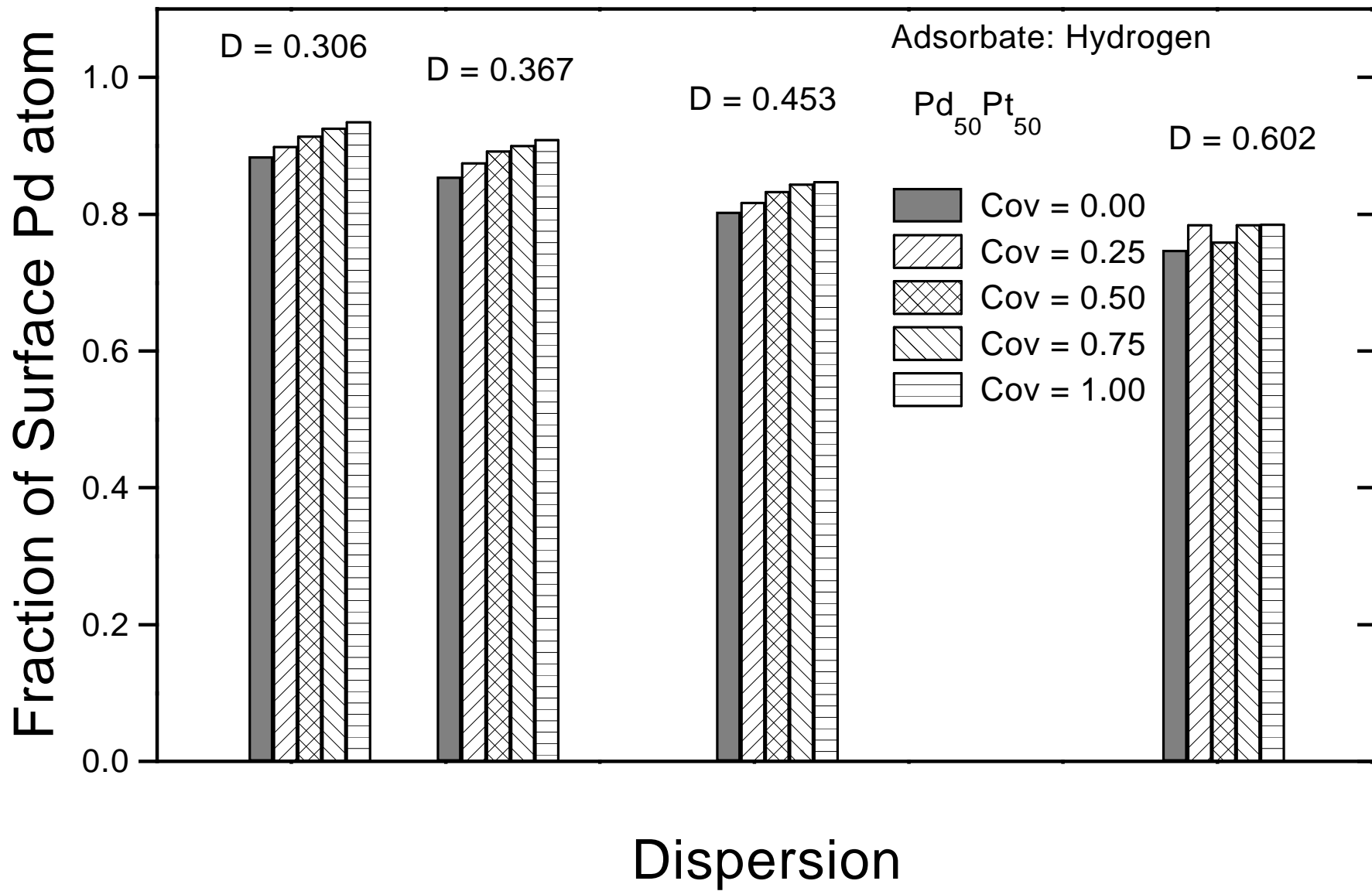


Fig. 4a  
Menon + Khanra

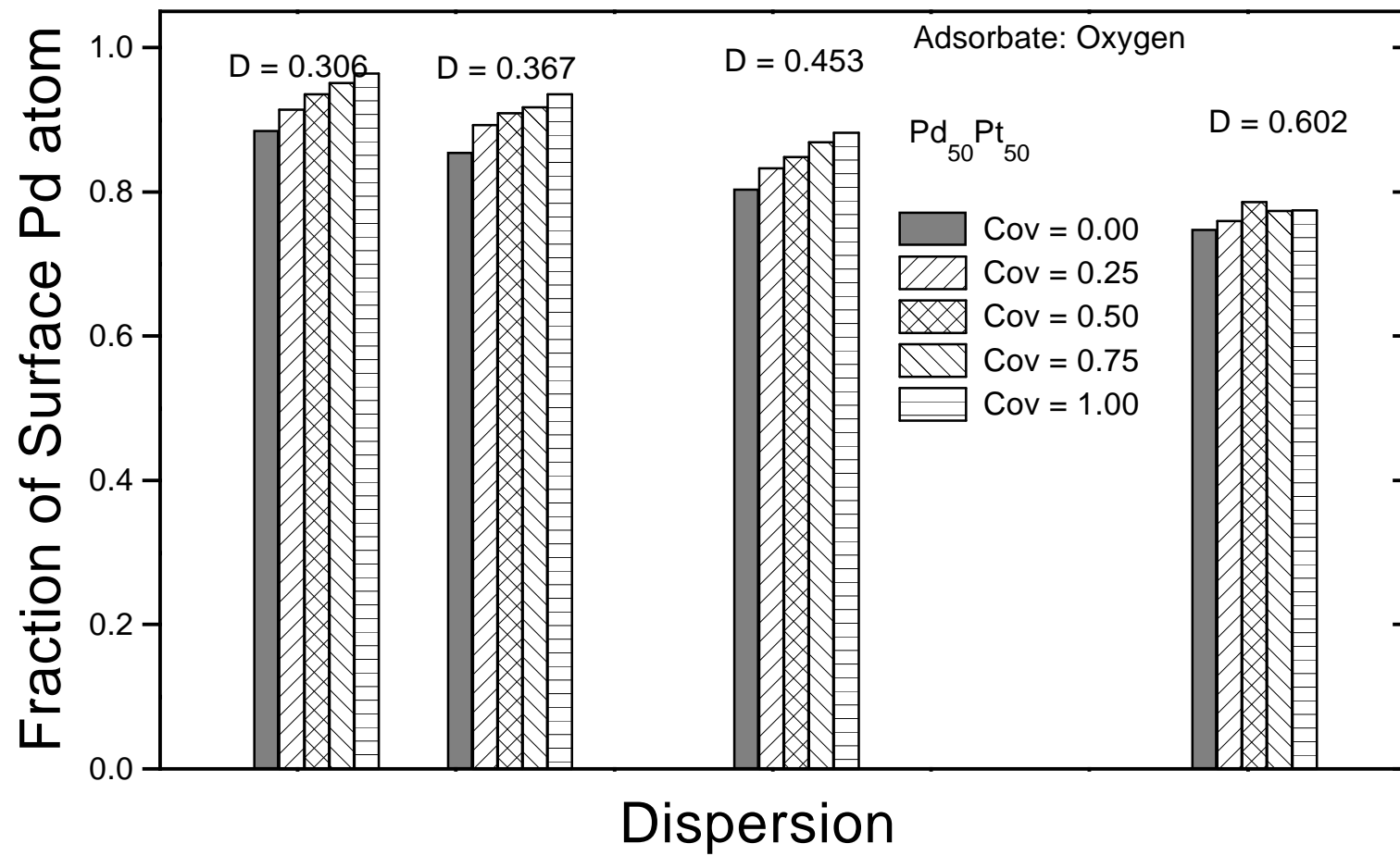


Fig. 4b  
 Menon + Khanra

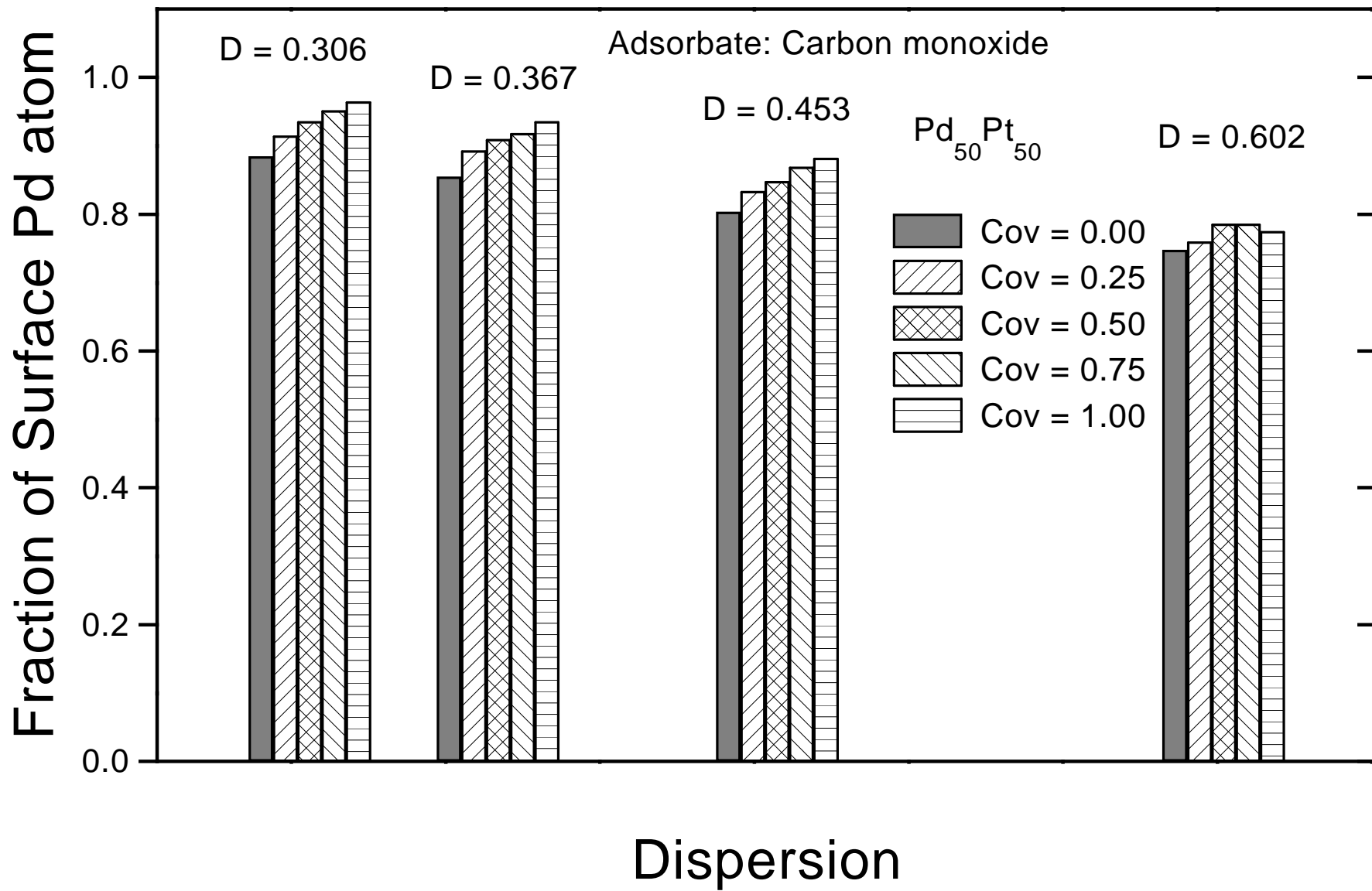


Fig. 4c  
Menon + Khanra

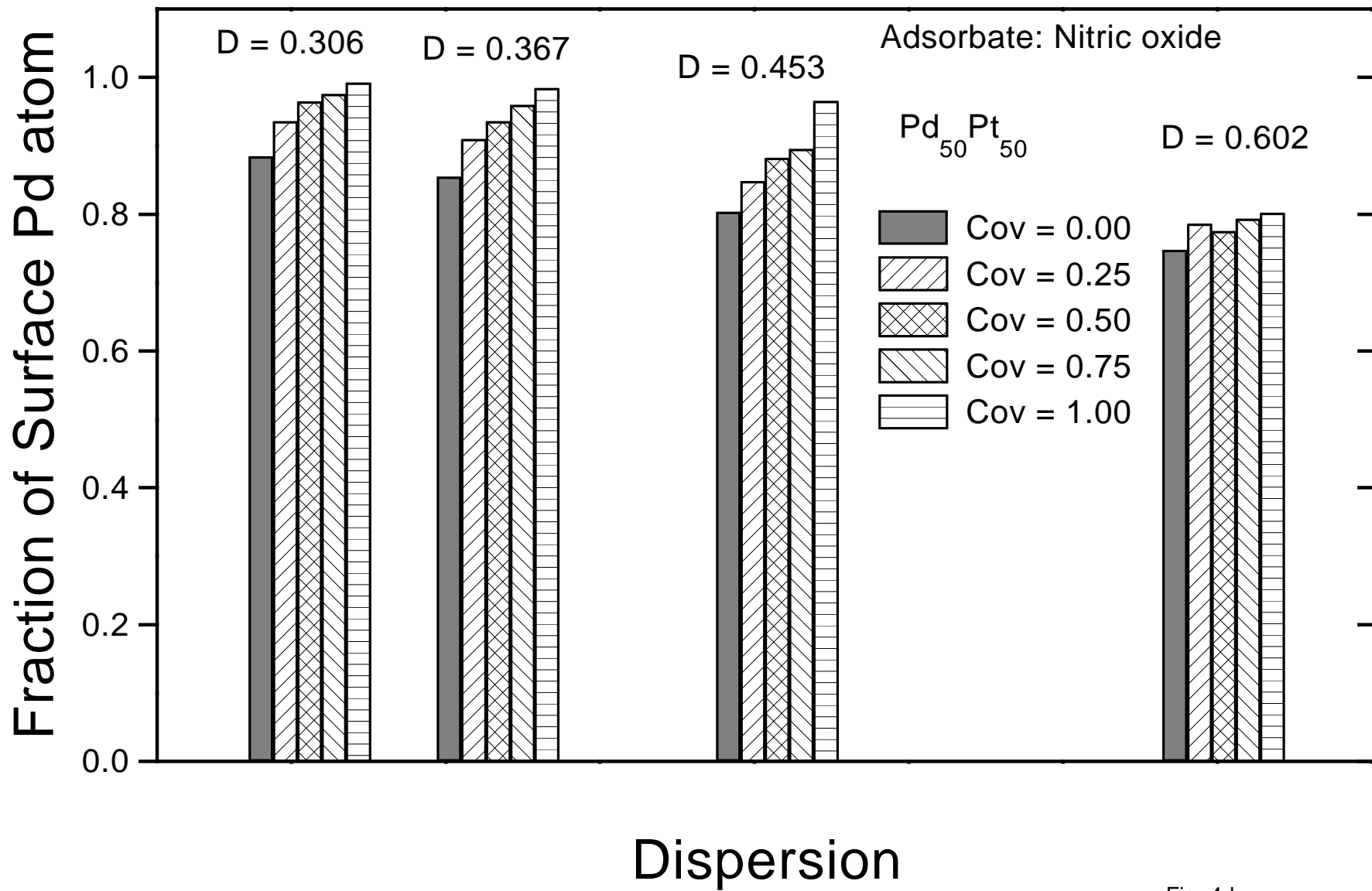


Fig. 4d  
Menon + Khanra

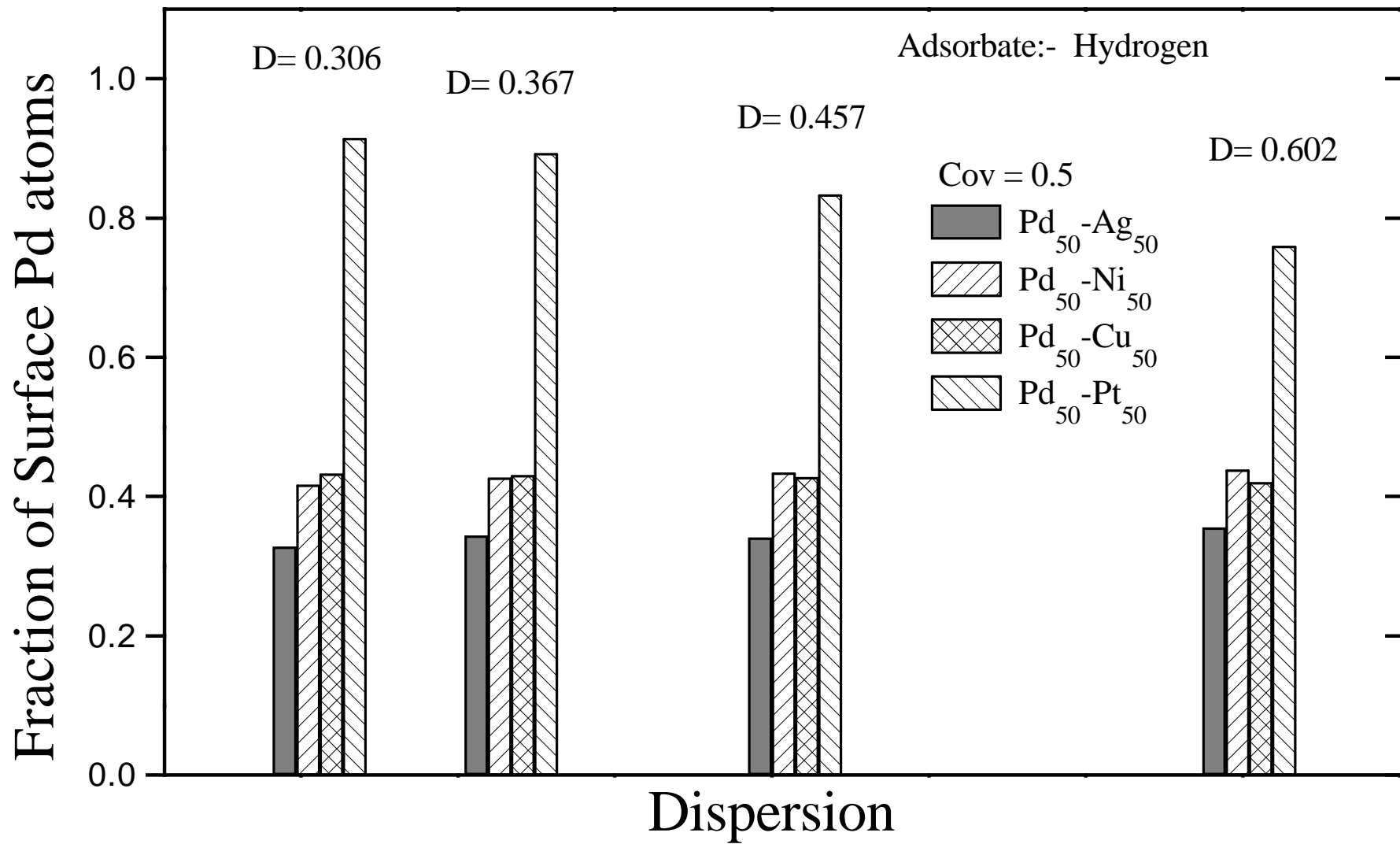


Fig. 5a  
Menon + Khanra



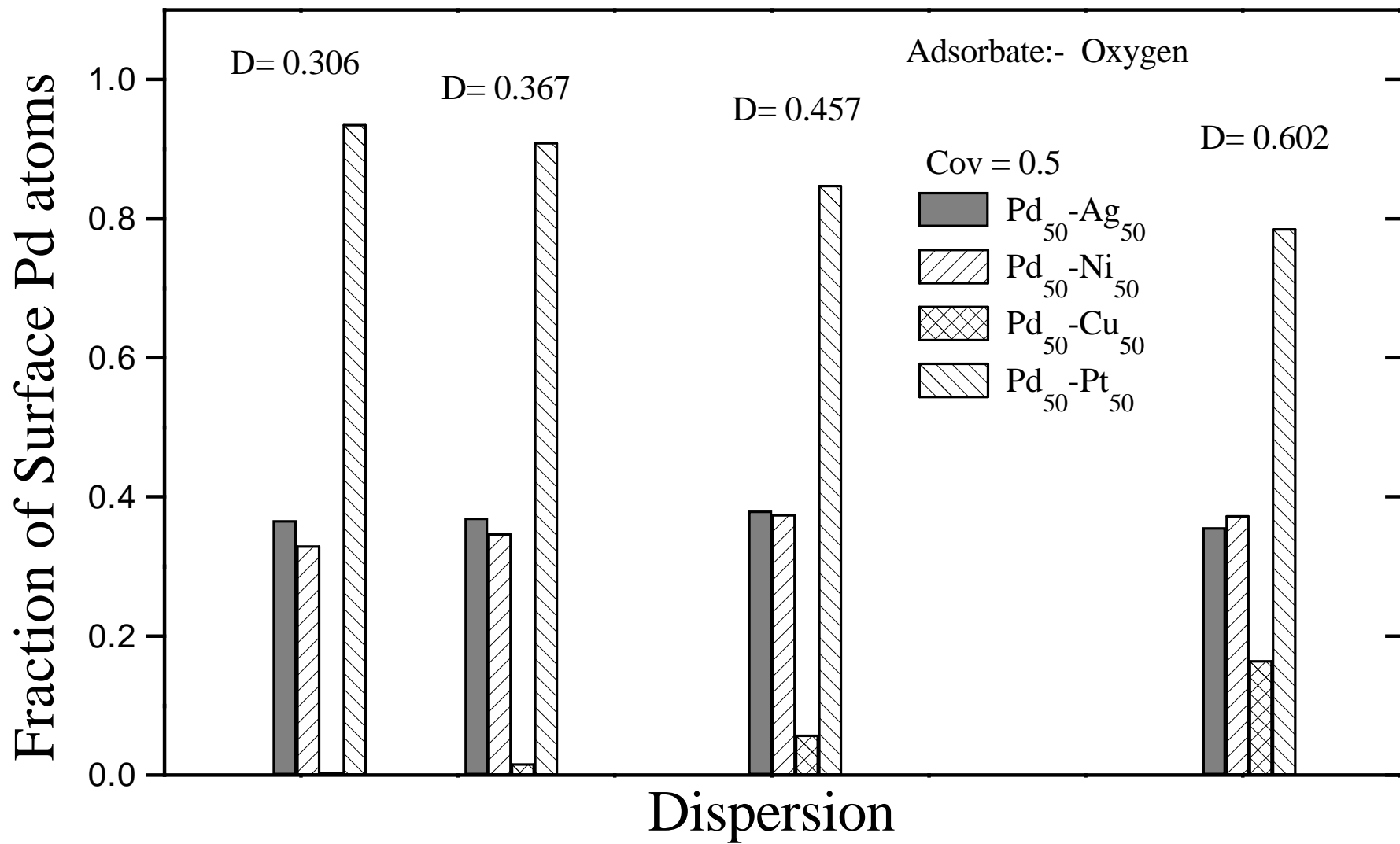


Fig. 5b  
Menon + Khanra

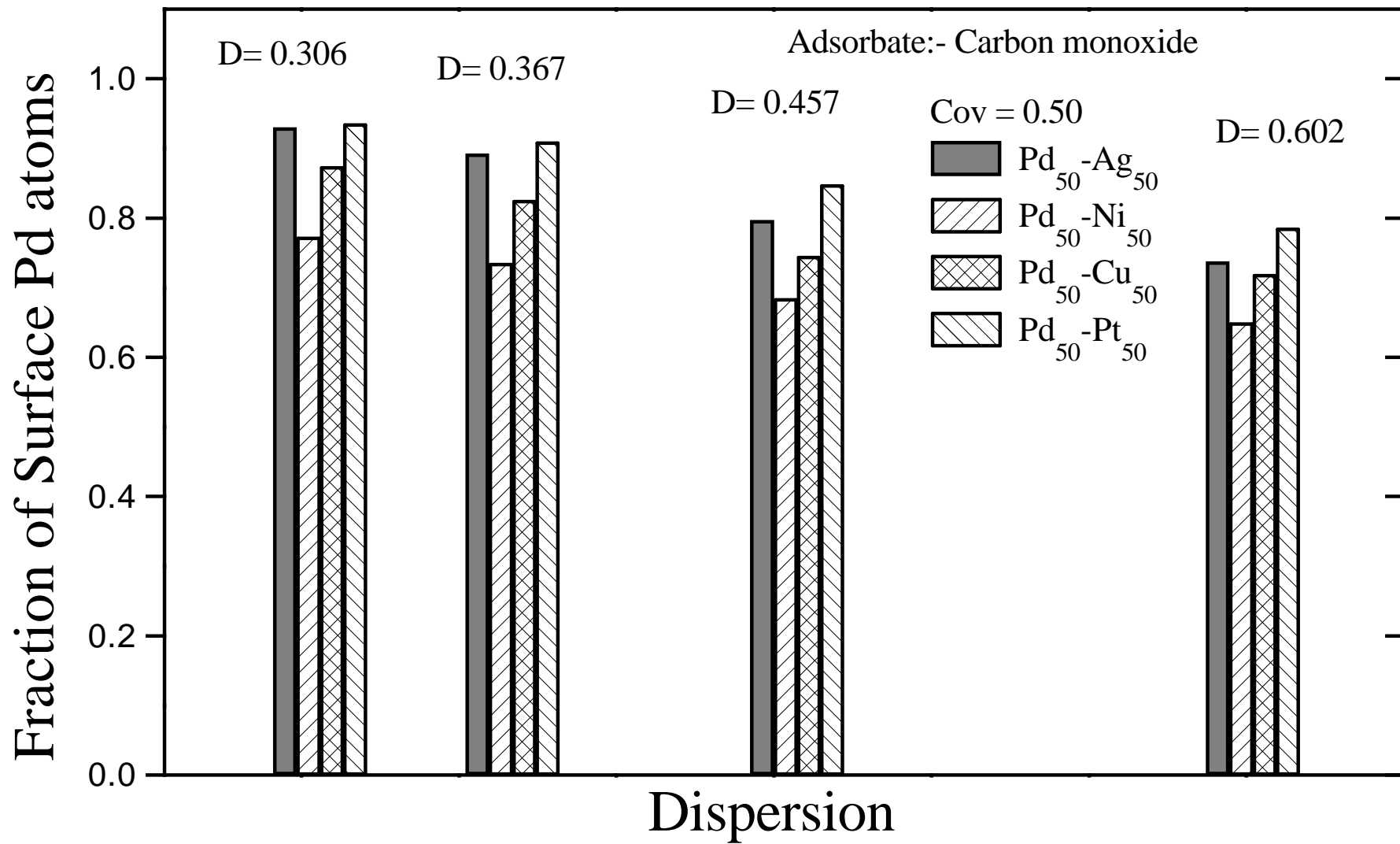


Fig. 5c  
Menon + Khanra

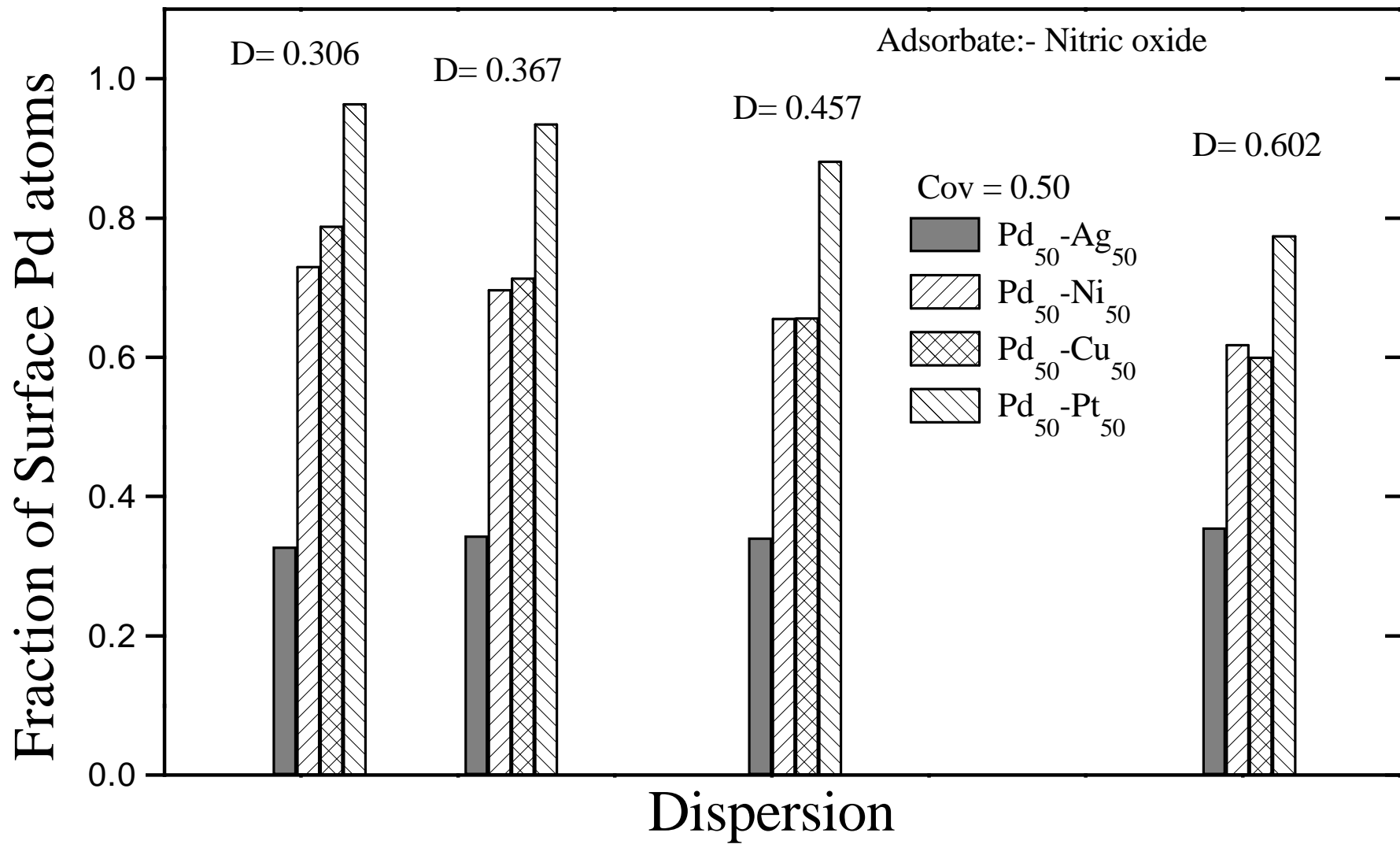


Fig. 5d  
Menon + Khanra

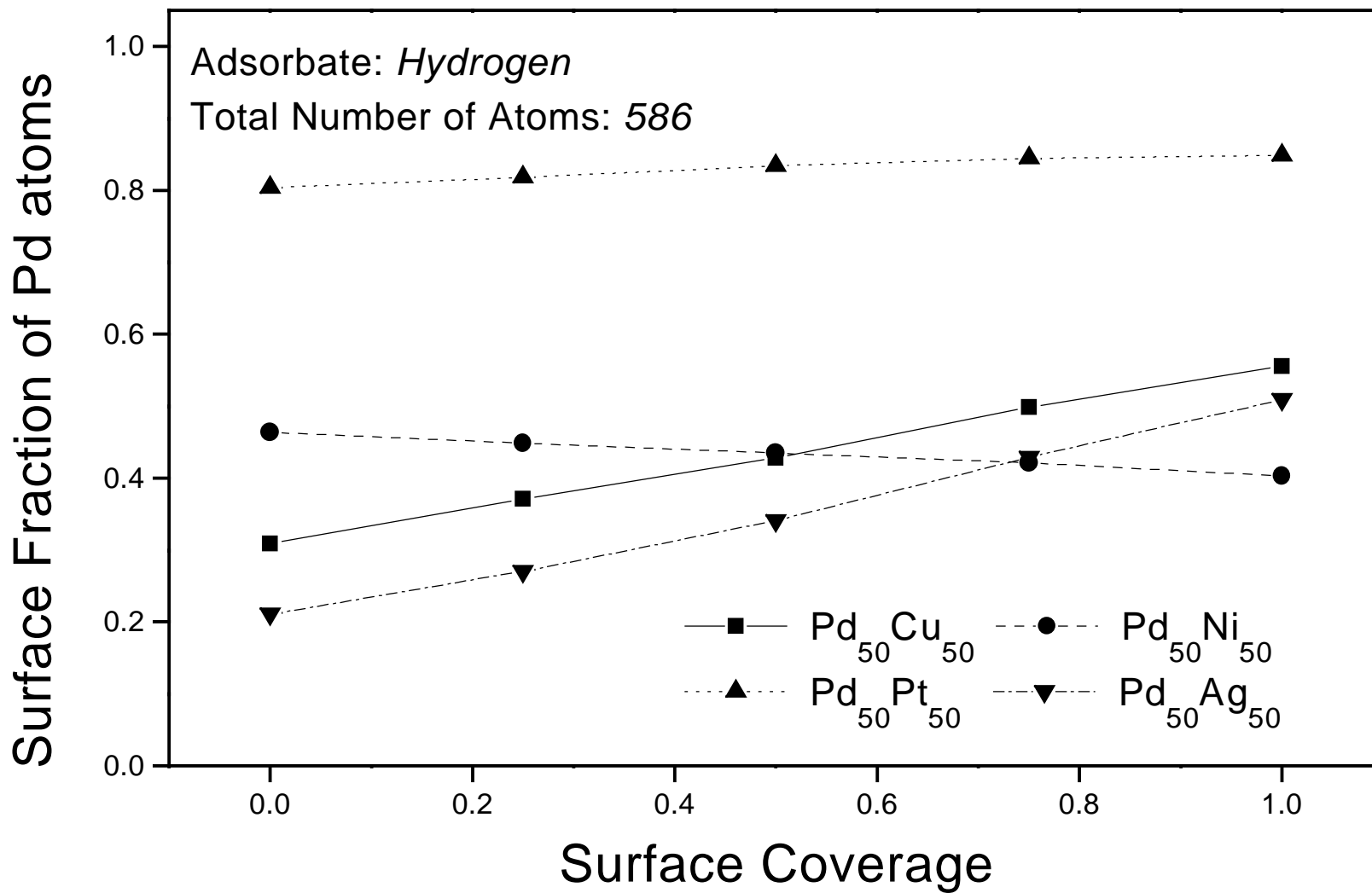


Fig. 6a  
 Menon + Khanra

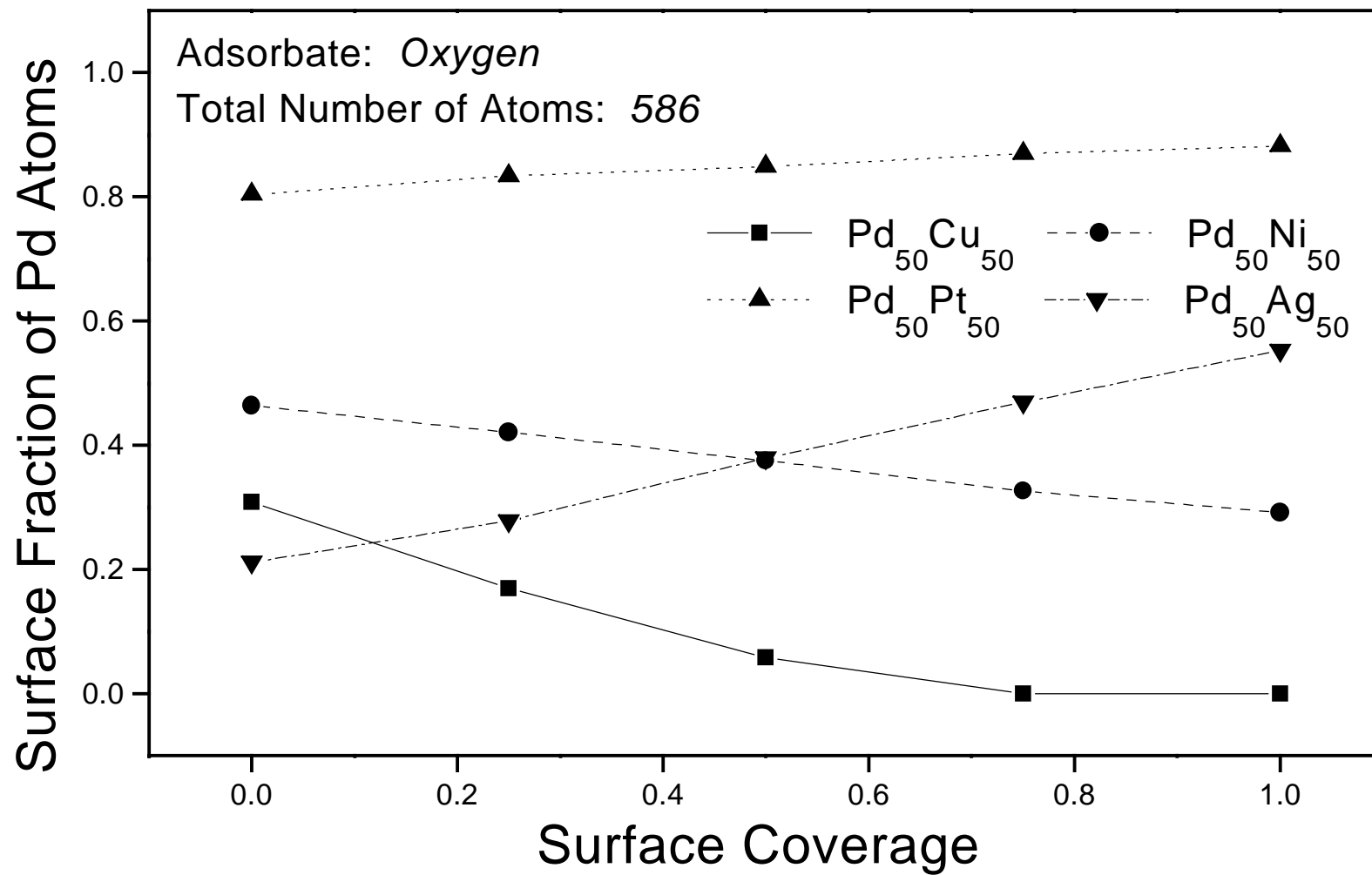


Fig. 6b  
 Menon + Khanra

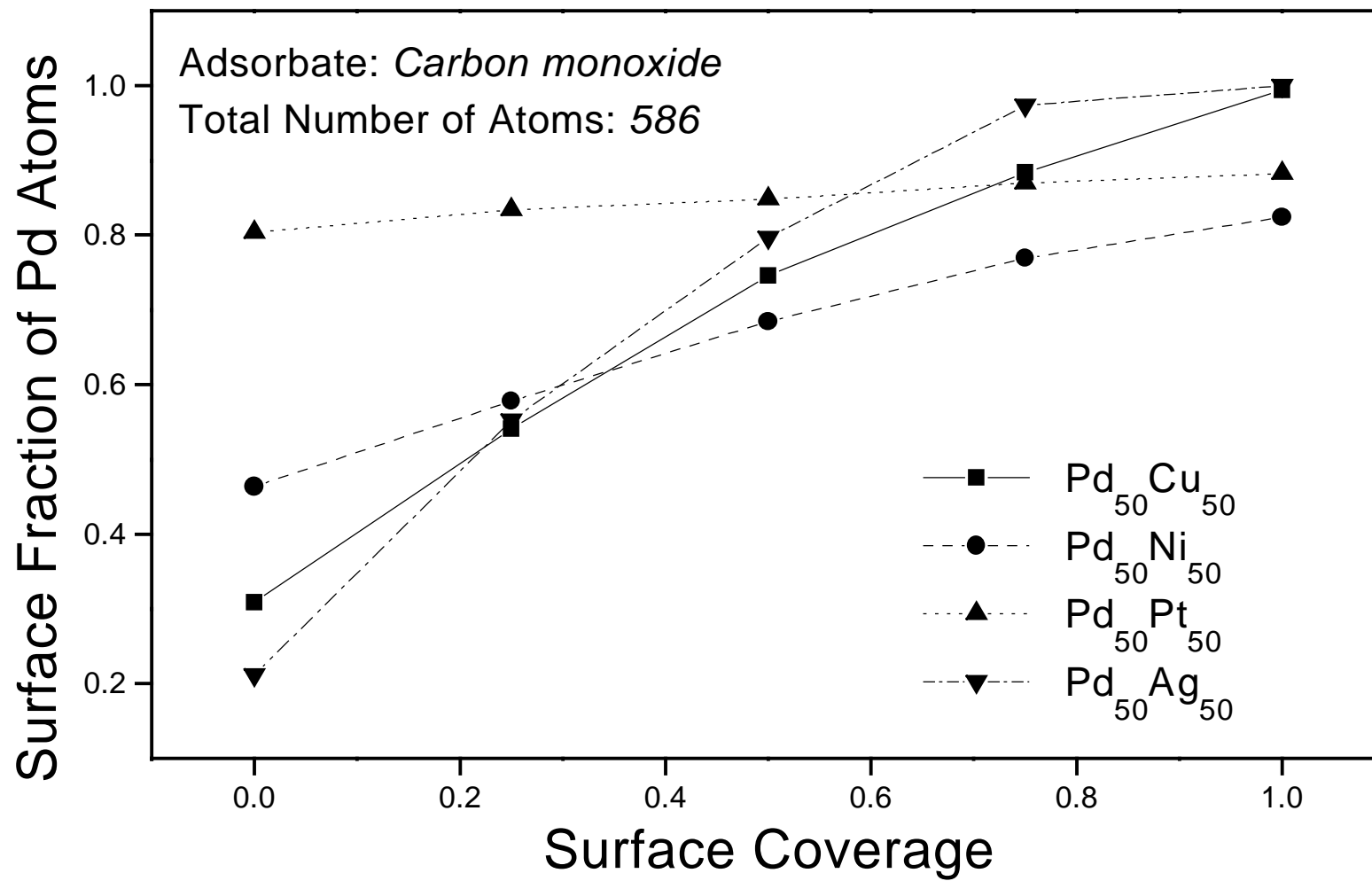


Fig. 6c  
 Menon + Khanra

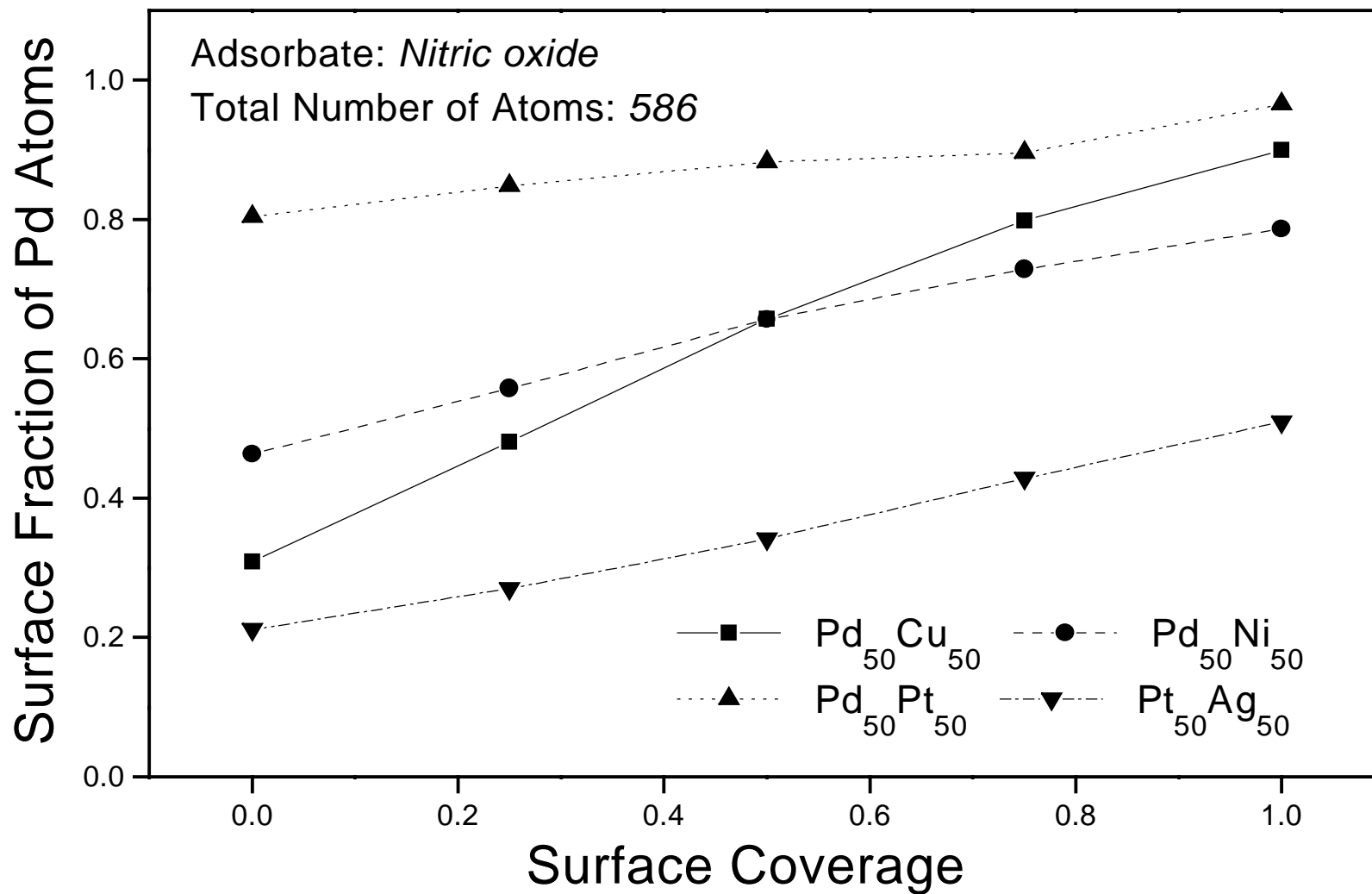


Fig. 6d  
 Menon + Khanra

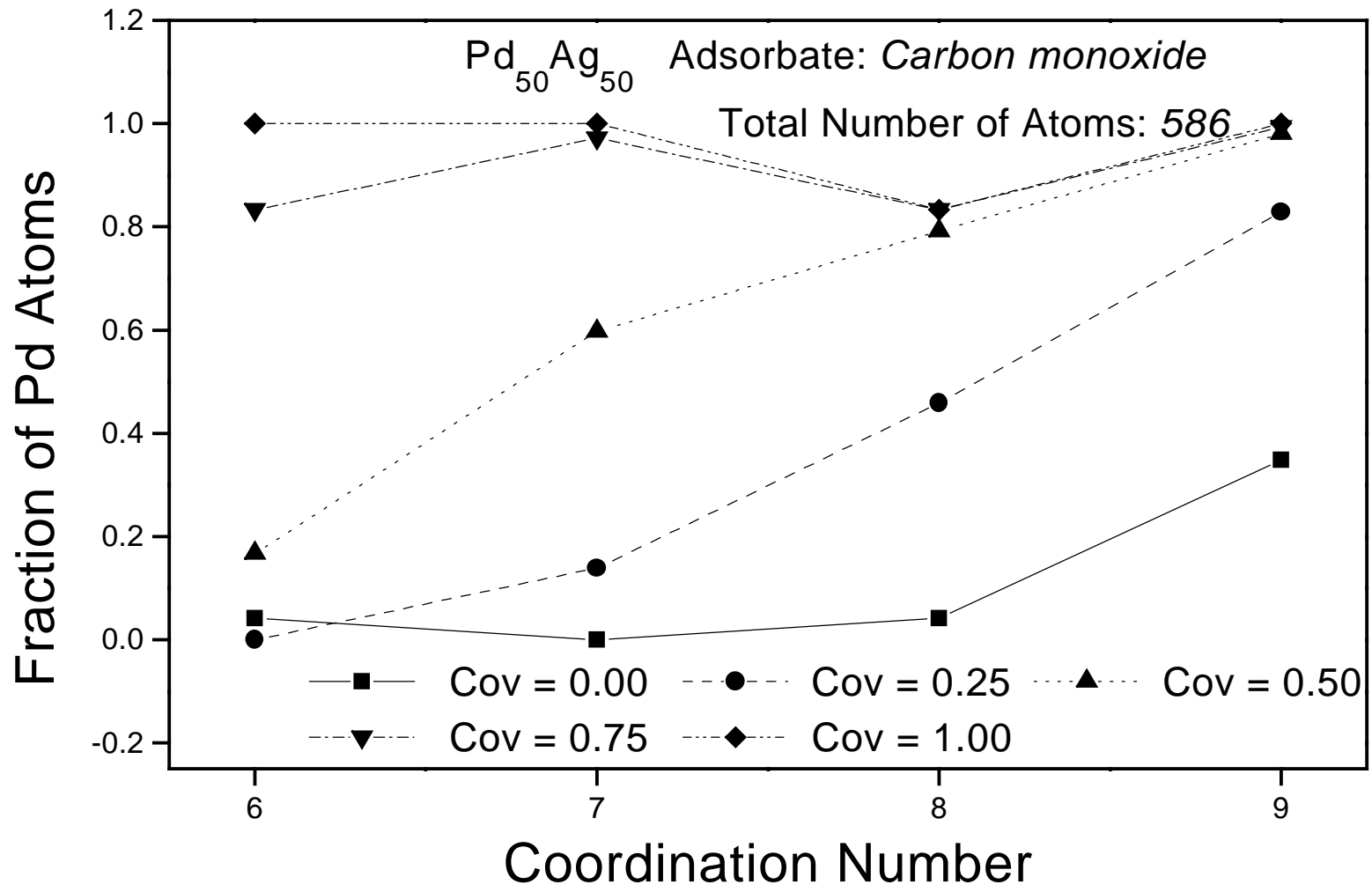


Fig. 7a  
Menon + Khanra



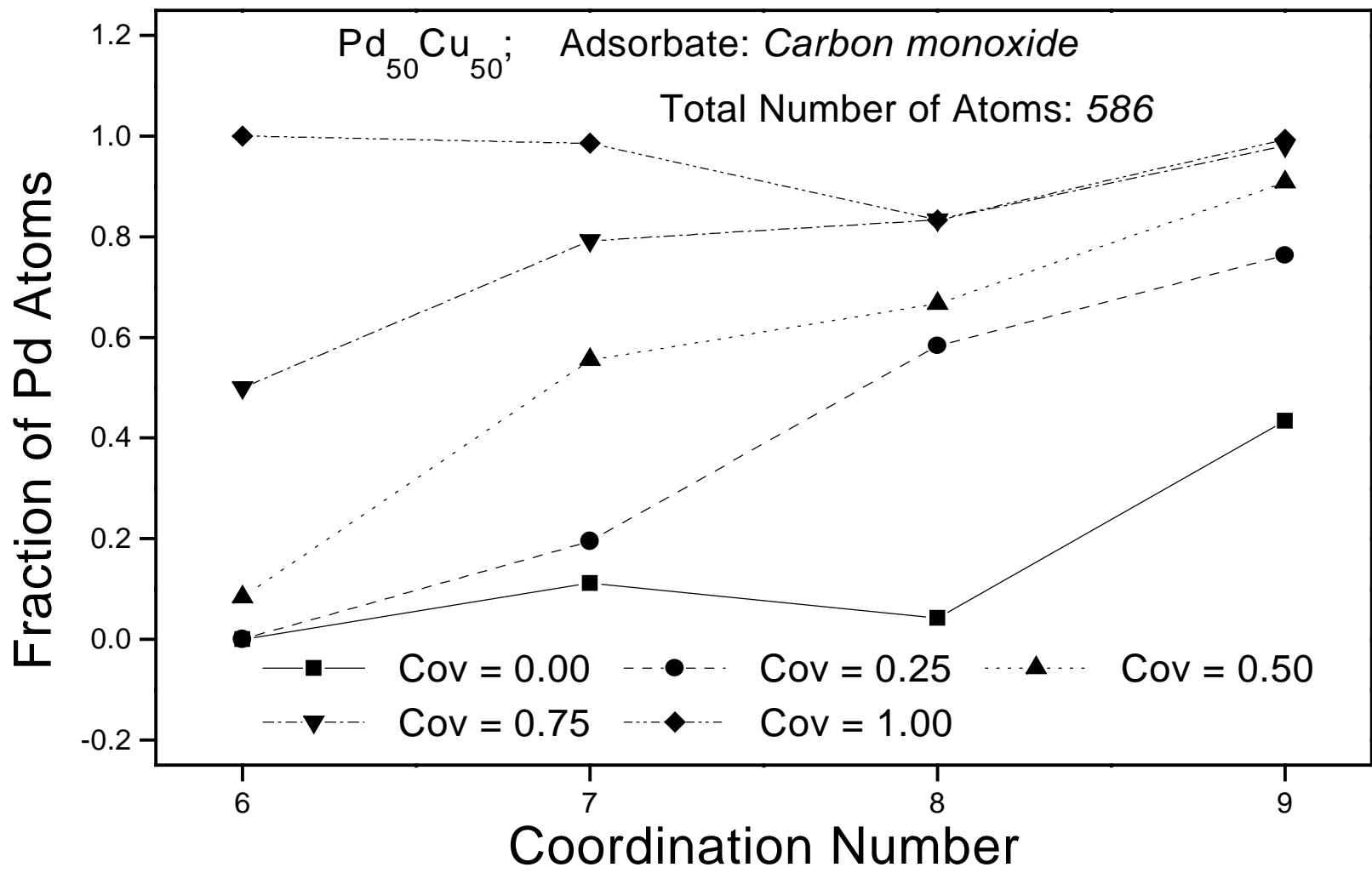


Fig. 7b  
 Menon + Khanra

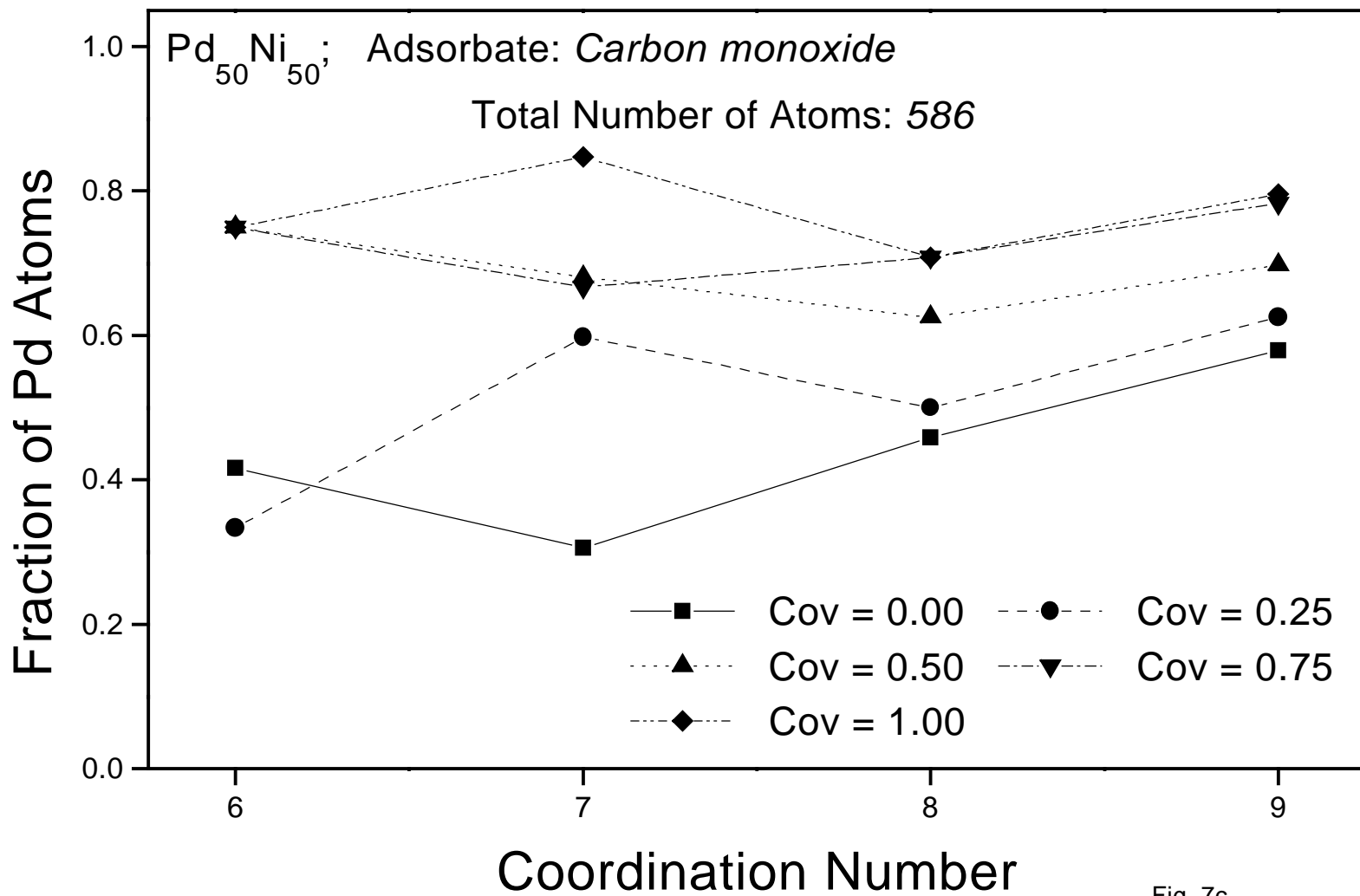


Fig. 7c  
 Menon + Khanra

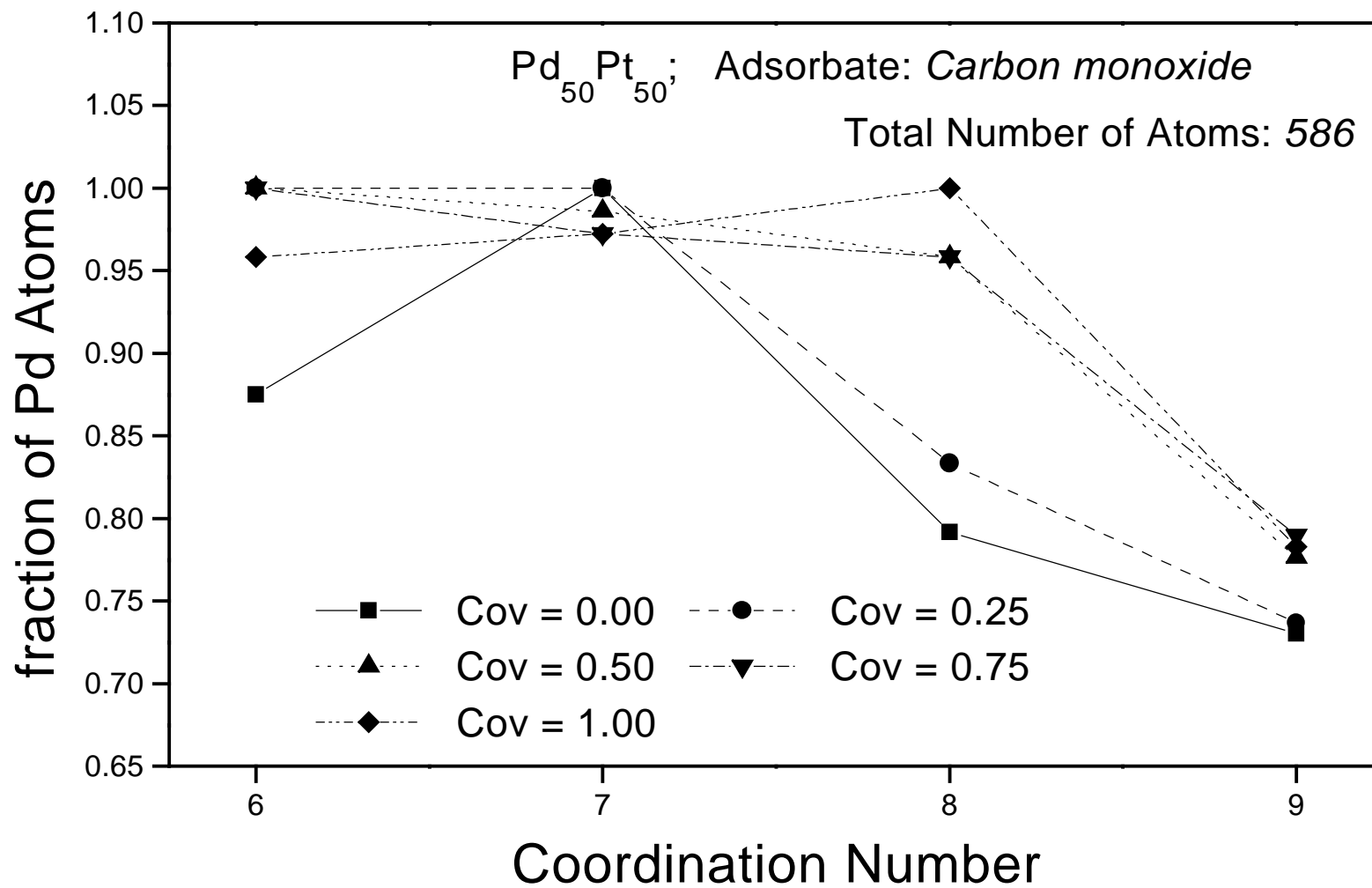


Fig. 7d  
 Menon + Khanra

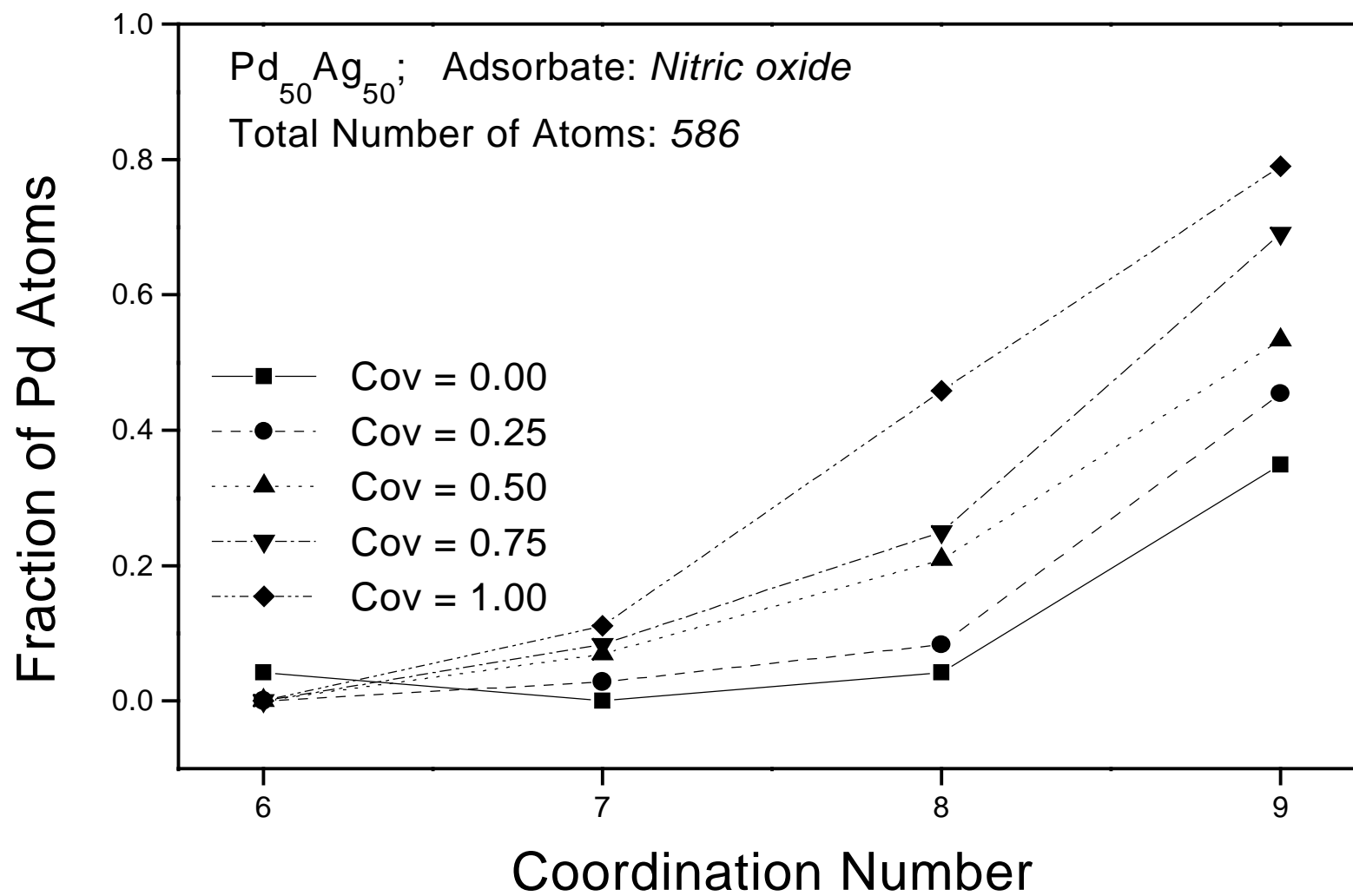


Fig. 8a  
Menon + Khanra

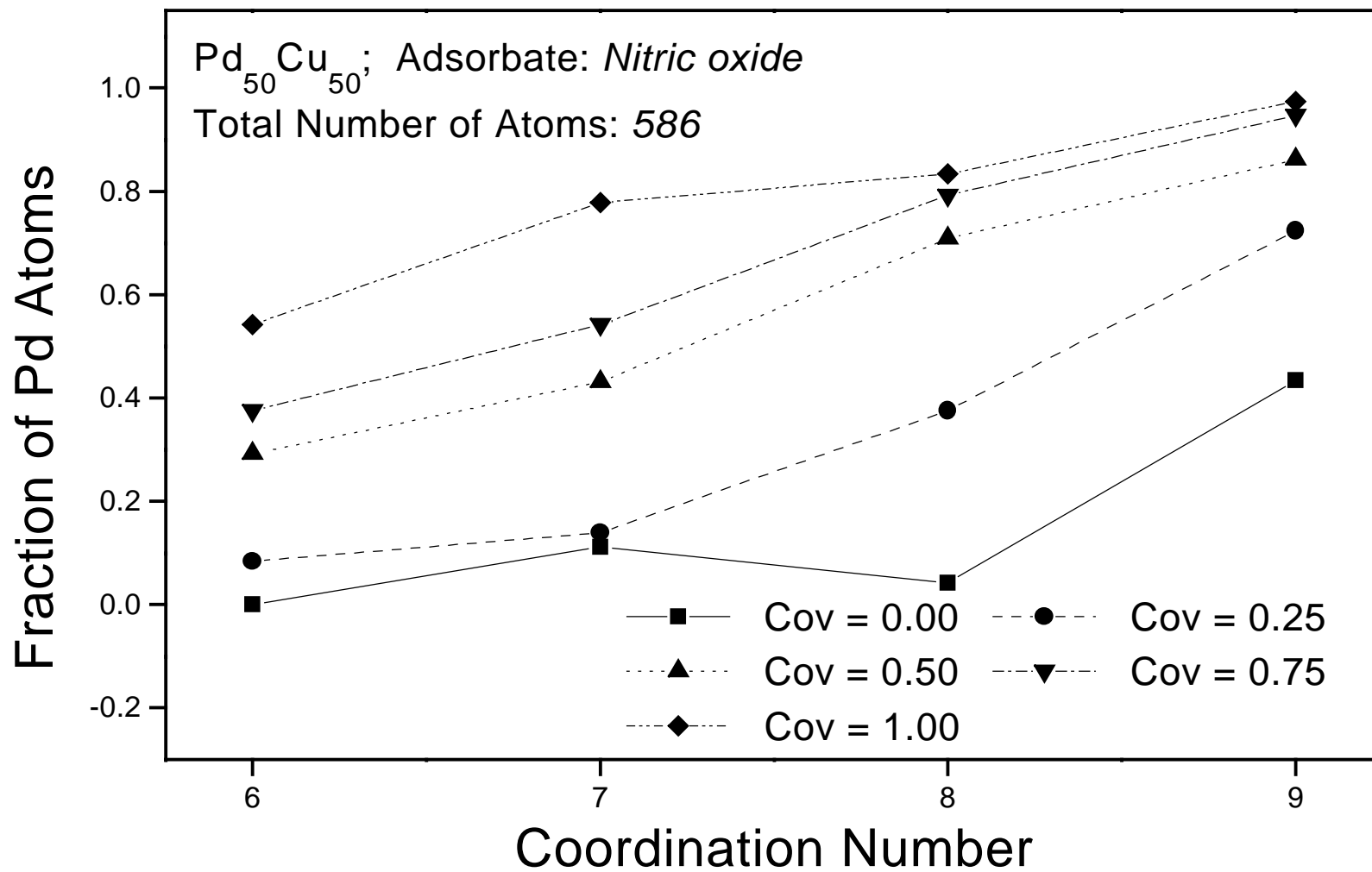


Fig. 8b  
 Menon + Khanra

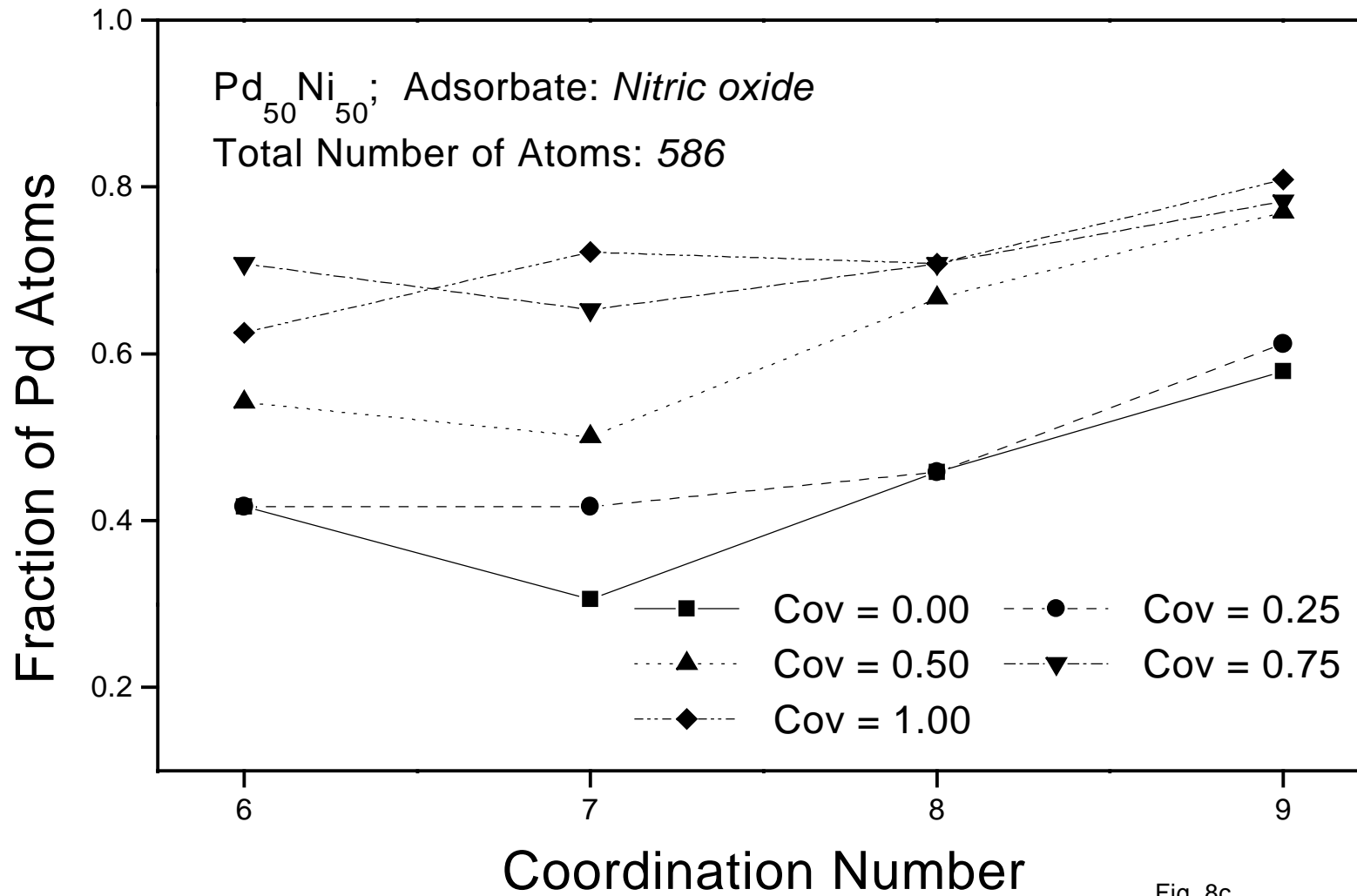


Fig. 8c  
Menon + Khanra

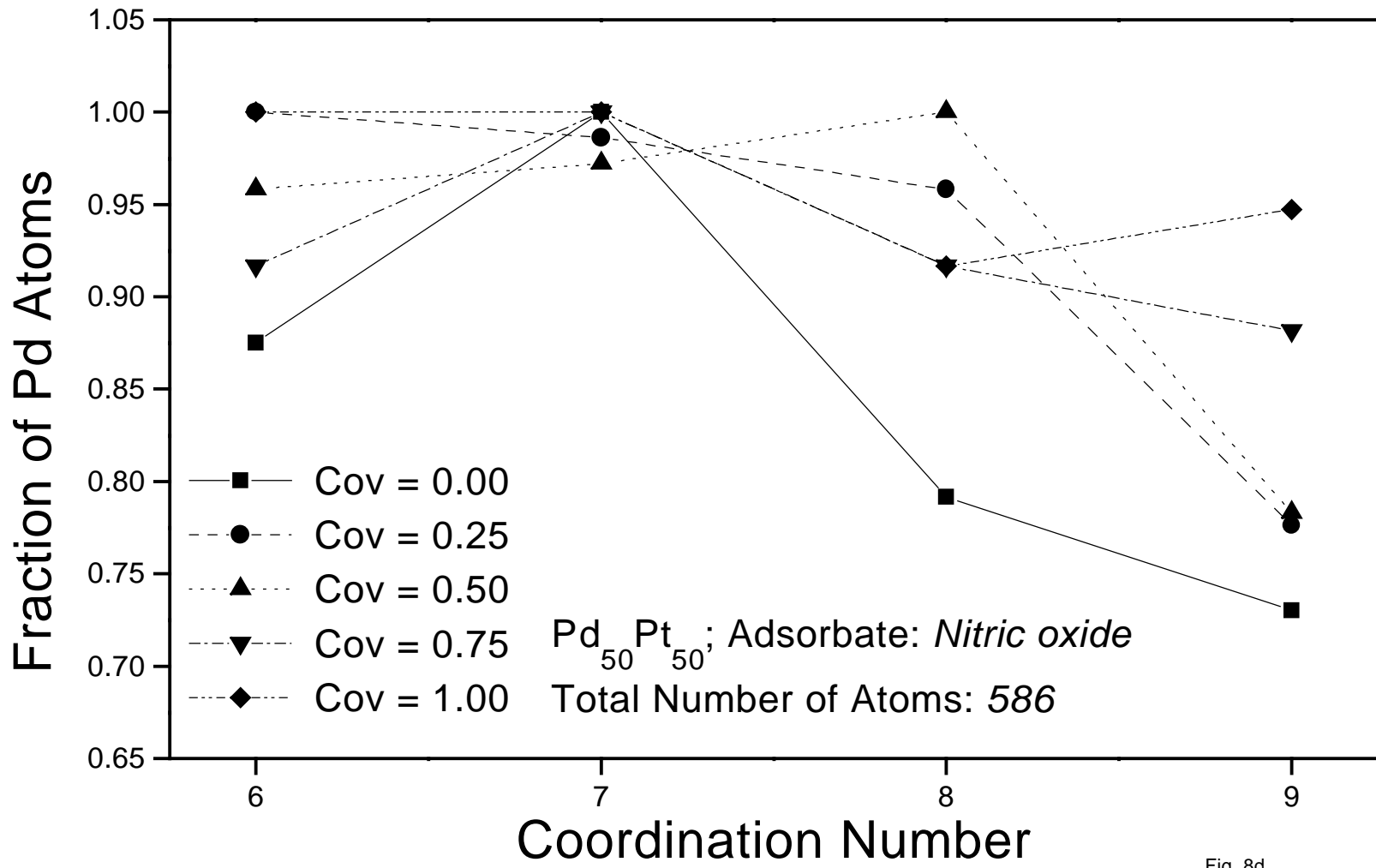


Fig. 8d  
Menon + Khanra

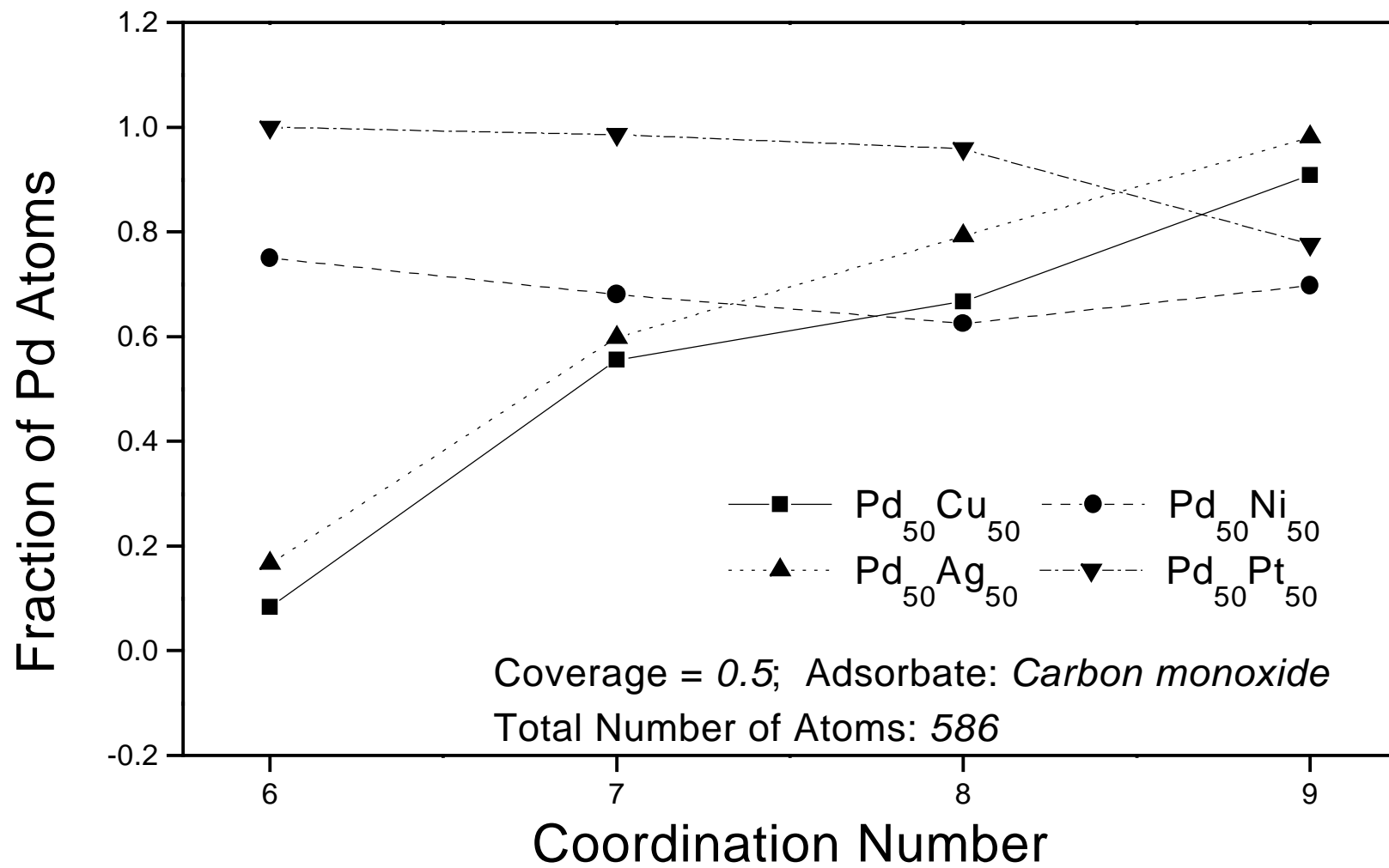


Fig. 9a  
Menon + Khanra



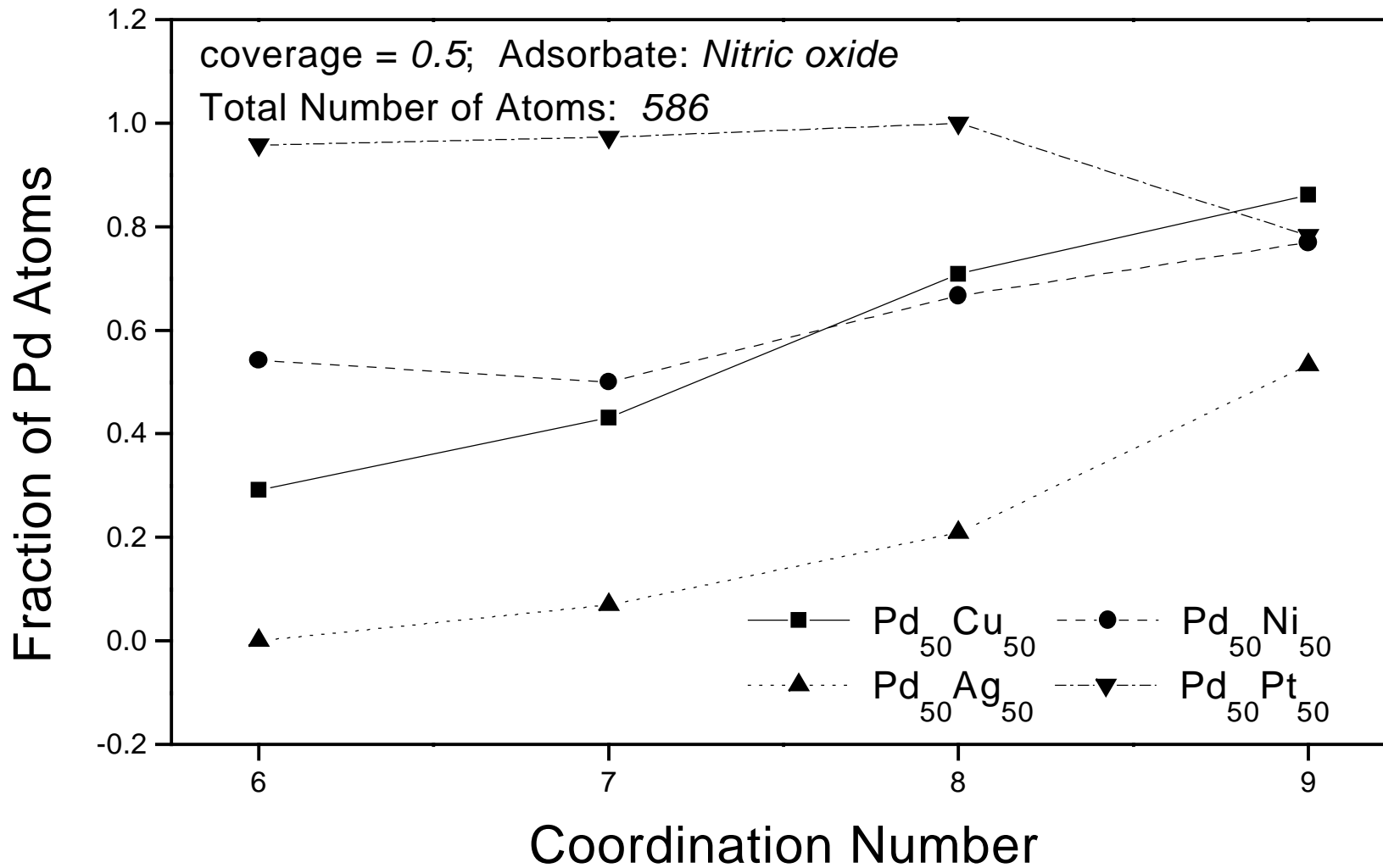


Fig. 9b  
 Menon + Khanra

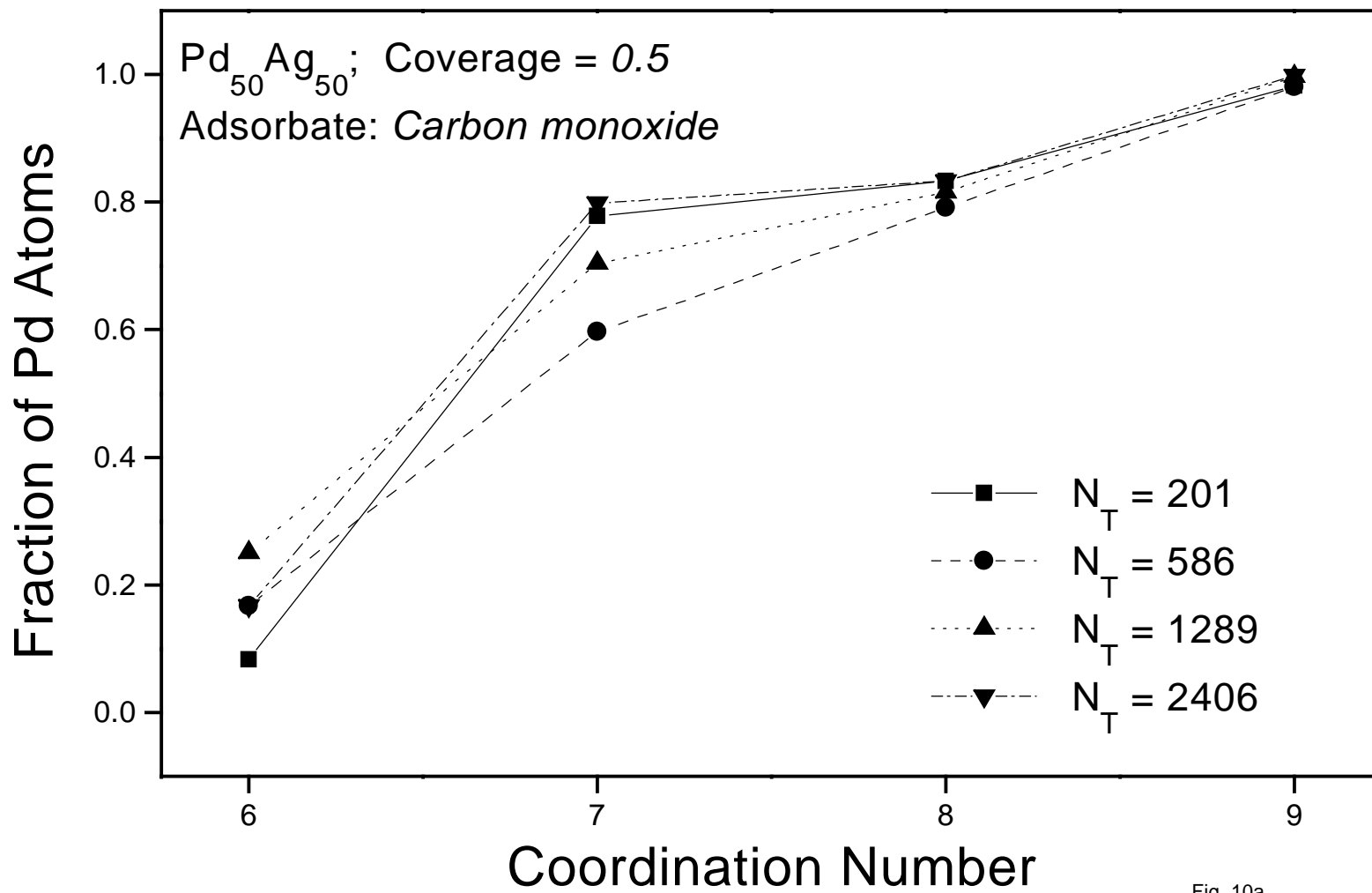


Fig. 10a  
Menon + Khanra

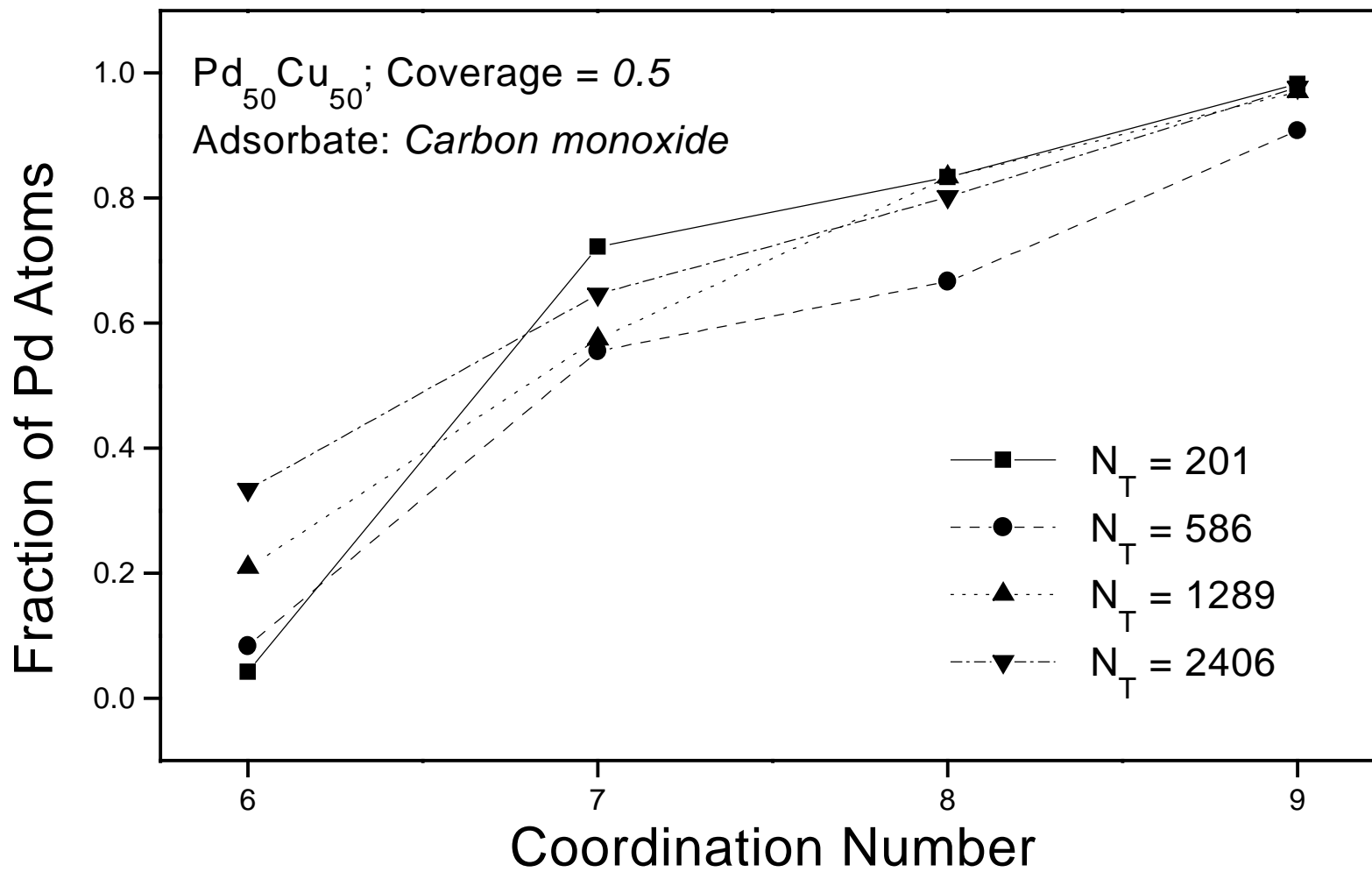


Fig. 10b  
Menon + Khanra

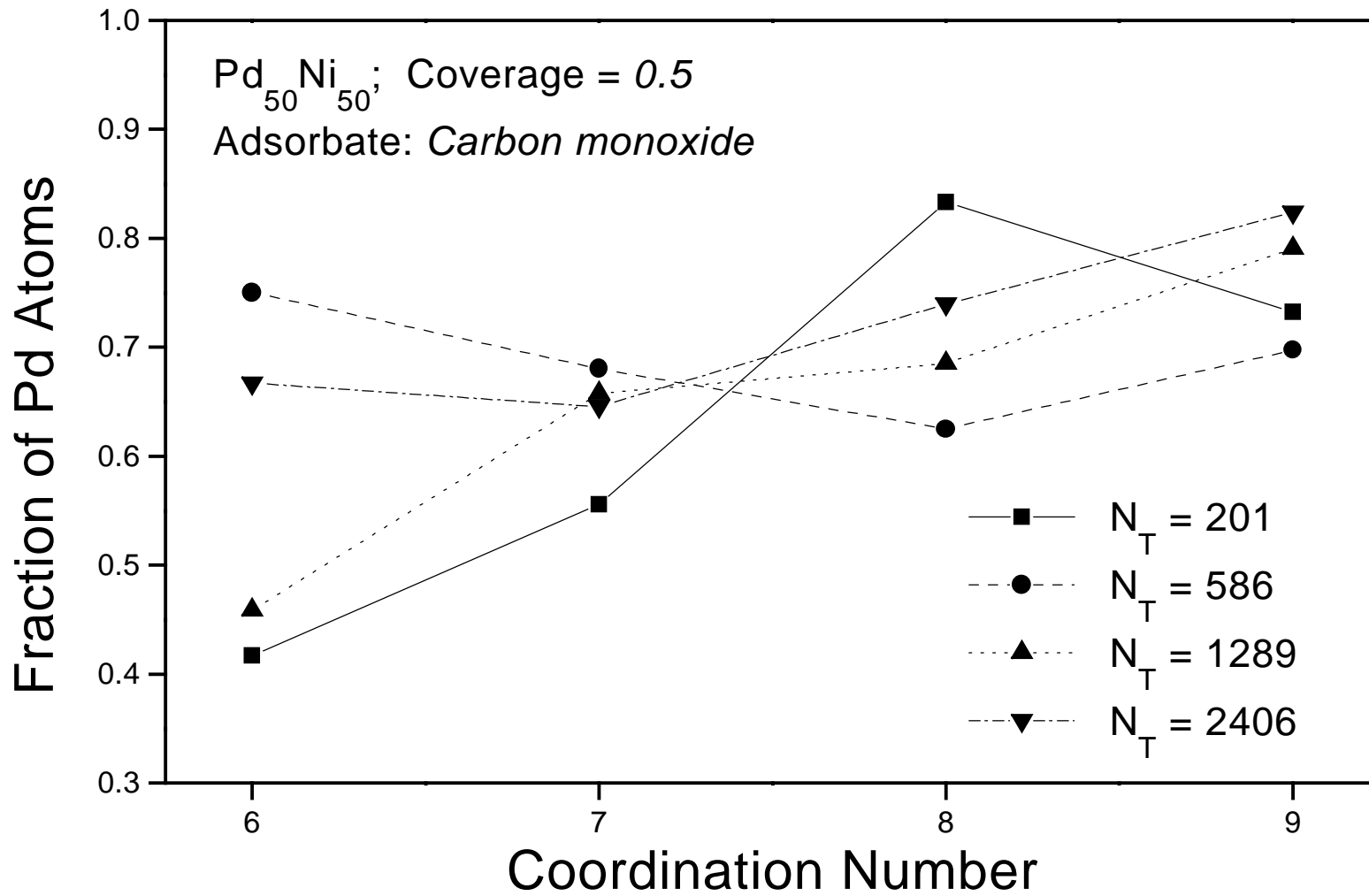


Fig. 10c  
Menon + Khanra

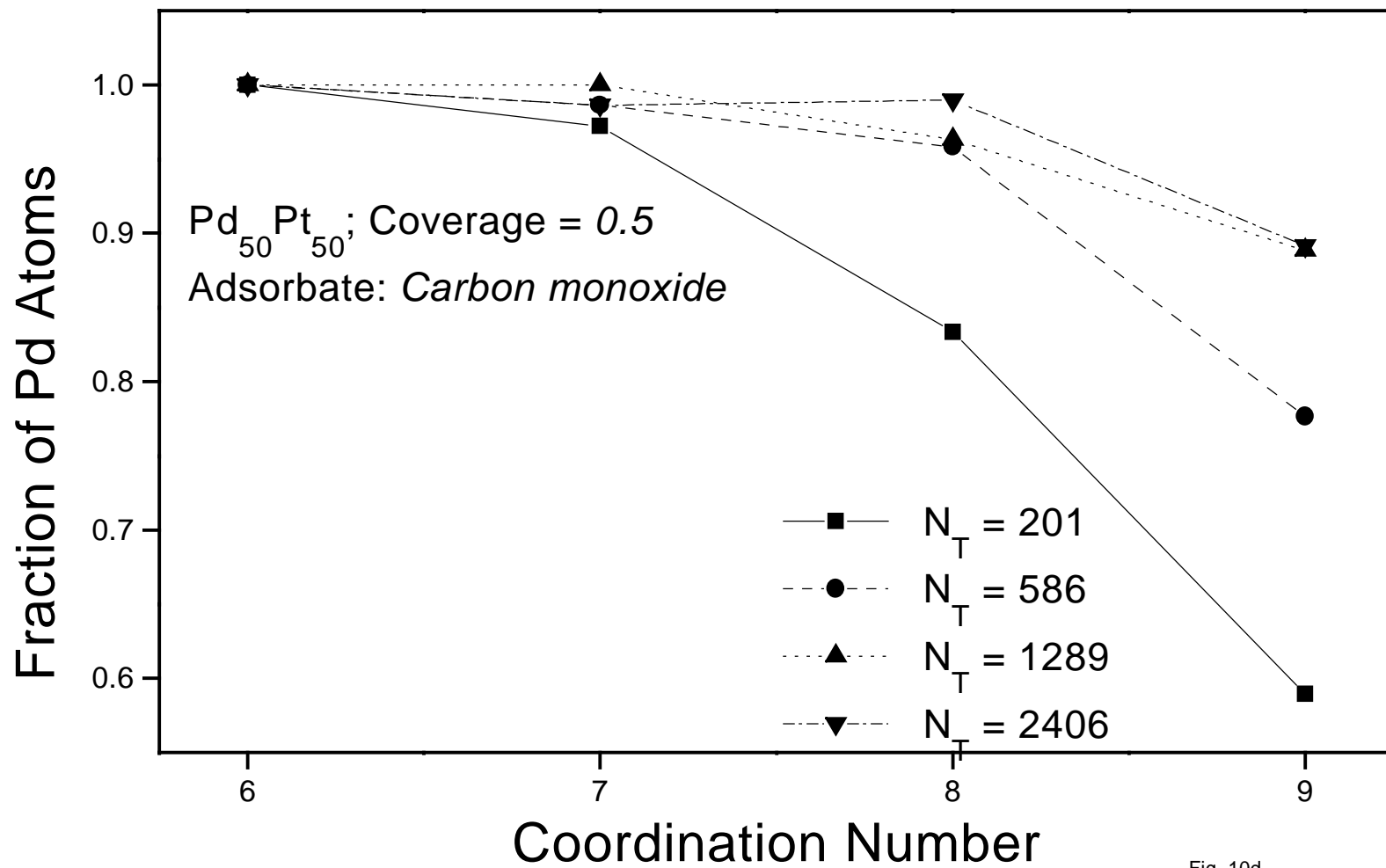


Fig. 10d  
Menon + Khanra